WMRC Reports
Waste Management and Research Center

Removal of Metallic Impurities in Chromium Plating Solutions by Electrocoagulation

S. B. Lalvani
Southern Illinois University

RR-92
April 2002
Electronic Version

About WMRC's Electronic Publications:

This document was originally published in a traditional format.

It has been transferred to an electronic format to allow faster and broader access to important information and data.

While the Center makes every effort to maintain a level of quality during the transfer from print to digital format, it is possible that minor formatting and typographical inconsistencies will still exist in this document.

Additionally, due to the constraints of the electronic format chosen, page numbering will vary slightly from the original document.

The original, printed version of this document may still be available.

Please contact WMRC for more information:

WMRC
One E. Hazelwood Drive
Champaign, IL 61820
217-333-8940 (phone)

www.wmrc.uiuc.edu

WMRC is a division of the Illinois Department of Natural Resources

Removal of Metallic Impurities in Chromium Plating Solutions by Electrocoagulation

Dr. S. B. Lalvani

Department of Mechanical Engineering and Energy Processes
Southern Illinois University
Carbondale, IL 62901

Prepared for

Illinois Waste Management and Research Center
One E Hazelwood Drive
Champaign, IL 61820

This report is part of WMRC's Research Report Series. Mention of trade names or commercial products does not constitute endorsement or recommendation for use.

TABLE OF CONTENTS

LIST OF FIGURES

LIST OF TABLES

ACKNOWLEDGEMENTS

The funding for this research was provided by the Waste Management and Research Center, Champaign, Illinois and the Materials Technology Center, Southern Illinois University-Carbondale, IL. Experimental assistance was provided by Kanchan Mondal, Ph. D. candidate and Dr. J. Pattanayak. Dr. Wiltowski provided help with ICP analysis. Dr. N. V. Mandich of HBM Electrochemical Co. provided valuable insights into this research. We also thank the staff at IWMRC for providing the technical reviews of our work performed.

ABSTRACT

Metallic impurities such as Ni, Fe, Cu ions in chromium plating solutions can be removed by electromigration followed by electrodeposition or coagulation using a porous pot, suspended in the bath and containing a lead cathode. In the same process, Cr(III) is oxidized to Cr (VI) at the insoluble lead anode leading to regeneration of the plating solution. Previous research and data from industrial operations have indicated the "porous pot" method could be a cost-effective and environmentally friendly method to continuously separate impurities and recycle spent chromium solutions. However, no data are available that relate the various concentrations of impurities to the extent and the rate of their removal. This investigation focused on the use of five suitable catholytes for the removal of impurities. Up to 60% nickel and 52% iron removal were observed in orthophosphoric acid and sodium monophosphate catholytes respectively. In addition to these two electrolytes, chromic acid appears to be a most suitable catholyte for purification when more than one metallic impurity is present in the spent solution. The rejuvenated chromium solution was used to make chromium deposits on various substrates. The deposits obtained from the rejuvenated solution were found to have microstructure and hardness and corrosion resistance properties similar to those obtained from freshly prepared solutions. These deposits had hardness and corrosion resistance properties far superior to those obtained from contaminated plating solutions. The kinetics of metal impurity removal and regeneration of hexavalent chromium were studied using a mathematical model developed in this study. The model was validated against experimental data.

1.0 INTRODUCTION

A typical spent hard chromium plating solution contains chromic oxide as anions of chromates, trivalent chromium and metallic impurities of nickel, iron, copper and zinc. A number of methodologies involving neutralization, adsorption, electrodialysis and ion-exchange have been reported for the removal of metallic impurities from chromium plating solutions. However, the above mentioned methods suffer from severe drawbacks in actual continuous practice. For example neutralization followed by precipitation of metals involves the use of a large volume of chemicals and results in the formation of sludge which is relatively difficult to handle and dispose off. In addition, this method works best when impurity concentration is relatively high. The problem with adsorbents lies in that they are expensive and generally non-selective. Electrodialysis suffers from the problems associated with membrane stability while ion-exchange methods are believed to be not very suitable due to their huge capital cost and volumes of effluents produced with regeneration [1-2]. A number of researchers have shown that upon the application of a DC electric field, the metallic cations of impurities present in the anode compartment migrate to the negatively charged cathode through a ceramic membrane (also called "porous pot") where they are concentrated [3-8]. Since the chromates are anions, they remain confined to the positively charged anode. Depending upon the solution pH, the impurities concentrated in the catholyte (i.e. electrolyte in the cathode compartment) as a result of electromigration are either electrodeposited on the electrode surface or precipitated. This method of separation is inexpensive and can be carried out rather easily in electroplating shops. According to Mandich et al [3] the advantages of this process over other methods for impurity removal are due to (i) simplicity of design

and operation, (ii) economy, and (iii) compactness. Generally, sulfuric acid is used as a catholyte, however, the use of this acid quickly leads to an increase in the solution pH upon the application of a DC field (due to hydrogen evolution at the cathode) which results in rapid precipitation of metals and hence the decrease of electrical conductivity. The increase in solution resistance leads to higher cell voltage demand (when operation is conducted at constant current) thus necessitating the cessation of operation, followed by cleaning of the cathode compartment and recharging with fresh sulfuric acid. Another possible disadvantage of using sulfuric acid is that sulfate anions could electromigrate to the positively charged anode and upset the required optimum sulfate to chromium ratio needed for hard chromium plating solution. It should be noted that sulfate ion acts as a catalyst in chromium plating [6]. The lead anode and lead cathode are used in this study. Lead forms an oxide layer on its surface that catalyzes the oxidation of trivalent chromium to hexavalent chromium. Therefore, lead cathodes and anodes are widely used in chromium plating industry.

The following is a list of various key mechanisms that govern the operation of porous pot subjected to the application of DC potential:

(a) Electromigration determines the movement of ions. The cations of Fe^{2+}, Ni^{2+}, Cr^{3+} and H^{+} are attracted towards the negatively charged cathode where they are concentrated inside the porous pot, whereas the anion such as chromates, dichromates, polychromates and sulfate (e.g. CrO_4^{2-}, $Cr_2O_7^{2-}$, $Cr_3O_{10}^{2-}$ and SO_4^{2-}) are driven towards the positively charged anode that is placed in the bulk of the spent plating solution;

(b) In addition to migration, the trivalent chromium ion, Cr^{3+} is oxidized to the hexavalent chromium (i.e. CrO_4^{2-}) at the anode compartment. Therefore, regeneration of hexavalent chromium is possible [8].

(c) Depending upon the electrode potential, specific electrochemical reactions such as iron and nickel electrodeposition, and hydrogen evolution at the cathode and oxidation of Fe^{2+} to Fe^{3+} at the anode can and do occur,

(d) Evolution of hydrogen at the cathode results in an increase of solution pH. The most common chemical reaction therefore in the porous pot (i.e. cathode compartment) involves precipitation of metals.

Even though the "porous pot" method may be an economical device for removing metallic impurities, its operation remains poorly understood. Mandich et al [3, 7] first described the chemical and electrochemical reactions as well the operational mode and suggested a qualitative explanation of reactions inside (i.e. cathode) and outside (i.e. anode) the pot. Some of the reactions that can occur in the cathode compartment are:

$$Me^{n+} + ne^- = Me^0 \quad (1)$$

$$2H_3O^+ + 2e^- = 2H_2O + H_2 \quad (2)$$

$$2H_2O + 2e^- = H_2 + 2OH^- \quad (3)$$

$$nH^+ + A^{-n} = H_nA \quad (4)$$

$$Me^{n+} + mOH^- = Me\,(OH)_m^{(n-m)+} \quad (5)$$

Where Me = Metal and, A = anion

The pH changes at the cathode inside the porous diaphragm occur are the result of reactions (2) and (3). Reactions (4) and (5) tend to decrease the rate of change of pH; reaction (4) accomplishes this when the buffer pH of the particular metal is reduced, and

reaction (5) when the solubility limit is reached and the hydroxide precipitation begins to act as a buffer.

If the catholyte does not contain buffering agents or complexing agents, the pH increases to high values upon the application of current. Some buffering action can occur due to the reaction of hydroxide with the metal ions present as the impurities. However, this reaction is less effective at buffering any pH change, especially as the solution becomes more purified and the concentration of metals decreases. There may be transient plateaus due to precipitation of Fe $(OH)_3$, Ni $(OH)_2$ etc., after which the pH will again increase. If the pH is maintained low enough, metallic impurities will be plated out at the cathode, rather than to form the hydroxides in the form of voluminous sludge.

In this study, the following tasks were undertaken:

(i) investigation of suitable catholyte(s) for the removal of impurities;

(ii) investigation of hexavalent chromium from trivalent chromium at the anode; and

(iii) study of properties of deposits prepared from rejuvenated plating solutions.

2. METHODOLOGY

2.1 Electromigration

A sketch of the batch glass reactors constructed is provided in Figure 1. The outside compartment contains 2,000 ml of anolyte while the inside compartment consists of a round porous ceramic diaphragm (porosity 40% and pore size 1 μm) with a capacity of 750 ml. Both anodes and cathodes are constructed out of lead grids. Other details of the reactor are provided in Table 1. The outside compartment (i.e. anode) consists of the impurity bearing (therefore designated as spent) hard chrome plating solution while the

side compartment (i.e. cathode) contains the selected solution (catholyte) in which the impurities are to be concentrated. Upon the application of a DC electric current (or voltage) the metal cations electromigrate to the cathode compartment where, depending upon the pH, temperature, current density and catholyte composition, they are either electrodeposited and/or precipitated. In a typical experiment, a known amount of metal impurities are added to the typical hard chromium plating solution which is made by dissolving 250 g of chromic acid powder in 1 L of water to which 2.55 g of sulfate ion as sulfuric acid have been added. Experiments involve the application of constant current at a temperature of 45 ^{o}C (temperature used in actual plating practice). Samples (5 ml) are drawn from the cathode and anode compartments at regular intervals. The metal concentration in solutions was determined using a Perkin-Elmer inductively coupled plasma spectrometer (ICP). The pH of the samples is also monitored. In addition, the voltage drop across the reactor is noted. Any sludge formed in the reactor is collected and analyzed.

2.2 Preparation of Anodes for Hexavalent Chromium Regeneration

The lead electrodes were made by cutting 3/32" thick sheets obtained by McMaster Carr (Chicago, IL) in to 10 cm X 1 cm pieces. The rest of the chemicals were supplied by Alfa Aesar (Ward Hill, MA). In accordance to the experimental conditions described by Vora et al [9], a passivating film was formed on the Pb surface by holding it in a 3 M H_2SO_4 solution for three hours at 0.4 V vs. the standard calomel electrode (SCE). The potential of this electrode was then spiked momentarily to 2.3 V vs. SCE to allow the creation of the nucleating sites for PbO_2 in the passive film. Finally, the electrode was

anodized at a constant potential of 1.7 V vs. SCE for a period of 8 hours. The Bi-doped PbO_2 layer was deposited on the PbO_2 coated lead from a bath containing 0.4 mM $Bi(NO_3)_2$, 0.12 M $Cu(NO_3)_2$, 10 mM $Pb(NO_3)_2$ along with 0.1 g/l of sodium dodecyl sulfate (SDS) in 1 M perchloric acid. Perchloric acid was used since the solubility of bismuth nitrate is high in the acid solution. A typical spent chromic acid bath contains Cr(III)/Cr(VI) in the ratio of 1:25. However, for the purpose of this investigation four different ratios of Cr(III) / Cr(VI) were synthesized from chromium sulfate and chromium trioxide while the sulfate concentration was maintained at 2.5 g/l. The total chromium metal concentration of the synthetic spent solutions was kept at 130 g/l, which approximately corresponds to a concentration of 250 g/l of CrO_3 used in hard chromium plating baths. The composition of the catholyte used in this study was identical to that of the anolyte in order to avoid the occurrence of any concentration across the ceramic membrane prior to the application of an electric field. The electrochemical oxidation of Cr(III) was conducted in a divided electrolytic cell as shown in Figure 2. The design parameters of the electrochemical cell are provided in Table 2. The analysis of the solutions at different times in both the cathode and the anode chamber were analyzed for the Cr(VI) content with an Ion Chromatograph (Dionex Corp, Sunnyvale (CA), Model # DX 500). The ion chromatograph was equipped with a conductivity cell (CD 20) and the Cr(VI) content was measured based on the conductivity in μSiemens. The column used was a CS5A - 4 mm column. The total chromium was measured using a Buck Scientific 210 VGP Atomic Absorption Spectrophotometer.

Table 1. Reactor Details (Sketch as in Figure 1)

Anode compartment	
Outer Diameter:	16.5 cm
Inner Diameter:	16.1 cm
Height:	25.0 cm
Thickness:	00.2 cm
Lead Anode Area:	1,922 cm^2
Cathode compartment	
Outer Diameter:	9.62 cm
Inner Diameter:	8.42 cm
Height:	19.80 cm
Thickness:	00.60 cm
Lead Cathode Area:	837 cm^2

Table 2. Physical specifications of the reactor for regeneration of hexavalent chromium. The explanation of the terms is provided in nomenclature

A_p (m^2)	$5.07 * 10^{-4}$
A_a (m^2)	$16 * 10^{-4}$
A_c (m^2)	$17.59 * 10^{-4}$
V_a (m^3)	$0.35*10^{-3}$
V_c (m^3)	$0.15 * 10^{-3}$
σ_1 (m^{-1})	1.45
σ_2 (m^{-1})	3.38
σ_3 (m^{-1})	4.57
σ_4 (m^{-1})	11.73

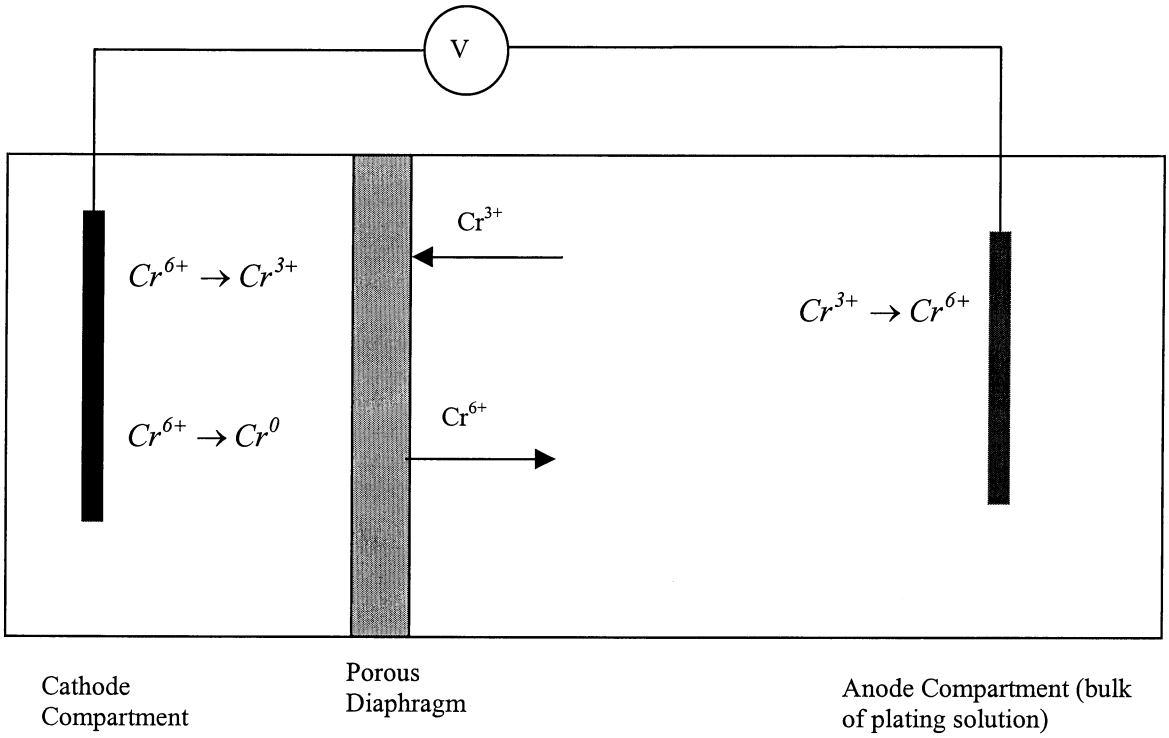

Figure 2. Schematic of the experimental setup for regeneration.

3. RESULTS AND DISCUSSION

3.1 Removal of Impurities

3.1.1 Catholyte Selection

In a set of preliminary experiments, a number of catholytes were examined for their pH values. The following rationale was used to investigate the selection of possible catholytes. Electrolytes containing the anion of Cl^-, SO_4^{-2}, or NO_3^- were not considered in this study because these anions could electromigrate to the anode compartment where the spent plating solution is placed. These anions are detrimental in that they either poison or overcatalyze the plating bath. The electrolytes were placed in the reactor

shown in Figure 1 and the electrical resistance across the reactor was determined. The data are presented in Table 3. The catholytes selected offer a wide variation in pH as desired. It is also interesting to note that when hard chromium plating solution is chosen as one of the catholytes, the electrical resistance is the lowest.

Table 3. pH and Electrical Resistance of Catholytes Under Invesitgation
The anolyte used is standard hard chromium plating solution (pH = 0.79)

Catholyte	**pH**	**Cell Resistance (milli-ohms)**	**Relative cell Resistance**
2.5M Chromic Acid*	0.79	0.077	1
0.5M Sodium Monophosphate (MSP)	4.45	0.252	3.3
0.5M Orthophosphoric acid (H_3PO_4)	1.18	0.291	3.8
0.5M Sodium Bicarbonate (baking soda)	8.34	0.364	4.7
0.5 Potassium Pyrophosphate (TPP)	11	0.402	5.2
0.5M Sodium Perchlorate ($NaClO_4$)	5.45	0.46	6.0

*Did not contain sulfate ion as it would migrate to the anode and overcatalyze the spent hard chromium plating solution.

The catholytes used included sodium monophosphate (MSP), potassium pyrophosphate (TPP), sodium bicarbonate, orthophosphoric acid, sodium perchlorate and the chromic acid solution. The catholytes chosen had a wide range of pH values, from very low to very high. The idea was to determine if the impurity removal is affected by

the pH of the electrolyte. At low pH, metal deposition is the preferred reaction while at high pH values, metal precipitation (as sludge) predominates. Both approaches have their merits and disadvantages.

3.1.2 Iron (Fe^{+2}) Removal

The source of iron used was ferrous sulfate. The total concentration of sulfate ion in the solution was controlled and maintained at 2.55 g/l. Figure 3 is a plot of total iron removal as a function of time. The experiments were conducted at 45°C and a current density of 7.8 A/ft^2. The data are reported for four sets of catholytes: sodium monophosphate, NaH_2PO_4 (0.5M); o-phosphoric acid, H_3PO_4 (0.5M); and sodium perchlorate, $NaClO_4$ (0.5 M), and chromic acid (2.5 M). The data show that up to 50% iron removal is possible in less than 5 hours when sodium monophosphate catholyte is used. However, the pH in the cathode compartment increased rapidly and at the end of experiment (30 hours) the pH had risen to 12.8 from an initial value of 3.7. Sludge formation was also observed in the cathode compartment which is consistent with the pH observations. About 27% iron removal was observed in the case of sodium perchlorate in 15 hours of operation while 21% iron removal was observed in the case of o-phosphoric acid catholyte. The use of o-phosphoric acid resulted in iron complex formation, which severely limited the conductivity of the solution (as evidenced by an increase in the cell voltage), and as a result the power consumption rose dramatically from 43 to over 100 watts over a period of 30 hours. However, when chromic acid was used as a catholyte, up to 28% iron removal was observed.

As compared to other electrolytes, the use of chromic acid as a catholyte led to a relatively lower amount of iron removal. At the anode, Fe (II) is oxidized to Fe(III). Ferric ions are known to form the negatively charged anions of iron-chromate complex [10]. This complex, because of its charge, is unable to electromigrate to the positively charged cathode compartment. Data reported in Figure 4 show that very small change in the solution pH is observed in the cathode and anode compartments when experiments are conducted for up to 24 hours at 7.8 A/ft^2 using chromic acid as a catholyte. In addition, the power consumption remained fairly constant (at about 32-39W) during the course of experiments. Thus, the hard chromium plating solution appears to be a good choice as a catholyte because of its buffering properties.

3.1.3 Nickel (Ni^{+2}) Removal

The source of nickel was nickel carbonate. Figure 5 is a plot of nickel removal vs. time. In the case 0.5M of sodium monophosphate (MSP), the metal removal increased almost linearly with time. Only a modest amount (14.6%) of nickel removal was achieved. In the case of o-phosphoric acid (0.5M), it is interesting to note that metal removal increased very rapidly at about 12 hours and up to 66% nickel removal is possible in 29 hours of operation. Also, the power consumption and pH of the catholyte remain relatively unchanged during the course of experiment. Thus, o-phosphoric acid appears to be a good catholyte for nickel removal. When 2.5M chromic acid (hard chromium plating solution minus the sulfate ion because the sulfate ion could migrate to the anode where it could overcatalyze the spent hard chromium plating solution) was used as a catholyte, up to 55% metal removal was obtained while the solution pH

remained almost unchanged, and the catholyte pH rose very slightly from an initial value of 0.58 to 1.27 for the experiment conducted at 7.8 A/ft^2.

The movement of metallic impurities of Ni^{2+} and Fe^{2+} across the ceramic membrane to the cathode occurs due to the application of DC field. These cations are attracted to the cathode which bears negative polarity. On the other hand, chromate ions are anions, therefore they are confined to the positively charged anode. However, hydrogen evolution occurs at the cathode due to reduction of protons ($2H^+ + 2e^- \rightarrow H_2$) resulting in an increase in the pH. At sufficiently high pH, metal (M) precipitation occurs according to the following equation:

$$M^{n+} + nOH^- \rightarrow M(OH)_n$$

The use of chromic acid as a catholyte did not result in a significant increase in the solution pH because chromic acid acts as a buffer. The data show that pH increase was accompanied by an increase in the cell voltage which presumably occurred due to a decrease in conductivity of the solution because of metal precipitation. In the case when chromic acid was used as a catholyte, an insignificant increase in solution pH occurred and thus no metal precipitation was observed. Therefore, should metal precipitation need to be avoided, the use of chromic acid as a catholyte is attractive especially for the removal of nickel impurities. Another advantage of the use of chromic acid as a catholyte is in that chromate ions move to the anode upon the application of voltage thus increasing the chromium concentration in the spent plating solution. Chromic acid is also inexpensive and it is readily available in the chromium plating shops.

3.1.4 Removal of Mixture of Impurities

A spent hard chromium plating solution was obtained from HBM Electrochemical and Engineering Company. The solution was found to contain 1.78 g/l of nickel and 17.4 g/l of iron. The solution was subjected to a current of 15.6 A/ft^2 at 45°C for a period of 24 hours. Chromic acid (2.5M) was used as a catholyte. The amount of metal removed vs. time plot is shown in Figure 6. The data shows a monotonic relationship between the amount of nickel and iron removal vs. time. Up to 46% of nickel and 24% iron removal was achieved in 24 hours. The power consumption was relatively low for the first ten hours of operation (85 W maximum). The results obtained are in accordance with the data on metal removal obtained from solutions containing single metal impurities. The residual amount of impurities from the plating baths could also be removed by carbonaceous adsorbents [11-12].

3.2 Characterization and Properties of Deposits

3.2.1 Evaluation of Composition of Deposits

Purification of the spent solution was carried out using the procedure described above. The solution entitled "Set 1" was collected from the HBM Electrochemical and Engineering Company and the solution entitled "Set 2" was synthesized in laboratory. The purification step involved the application of DC current of 14A (current density of 15.7A/ft^2) at 45°C. The data on metal removal are shown in Table 4-A.

Deposits were plated from solutions listed under Table 4-A. Plating was carried out using a constant current (of about 0.28 - 0.35 A/cm^2) at 45°C for an hour. The substrate (i.e. cathode) consisted of 304 stainless steel polished with #3 finish and of dimensions 6 cm x 1 cm.

Table 4-A Composition of Plating Solution

Experiments were conducted at 45°C using a current density of 15.7 A/ft^2

Solution	PH	Impurity	Spent Solution Concentration, mg/l	Rejuvenated Solution Concentration, mg/l	Removal (%)
Set 1	0.4	Iron	11,680	9,000	23.0
		Nickel	1,964	1,168	40.5
		Copper	9,408	5,720	39.2
Set 2	0.5	Iron	2,844	2,164	23.9
		Nickel	544	296	45.6
		Copper	2,356	1,308	44.5

Table 4-B Composition of Deposits Produced from Plating Solutions.

Sample	Iron (wt. %)	Nickel (wt. %)	Copper (wt. %)
Set 1			
a) Deposit from spent solution	0.48	0.12	0.23
b) Deposit from rejuvenated solution	0.12	0.05	0.07
Set 2			
a) Deposit from spent solution	0.13	0.04	0.07
b) Deposit from rejuvenated solution	0.10	0.04	0.07

The composition of the coatings was found by dissolving them in an acid and analyzing the solution using inductively coupled plasma spectroscopy (ICP). The composition of the deposits is reported in Table 4-B. It can be seen from the data that the deposits contain the impurities of iron, nickel and copper. The amount of impurities present in the deposits is a function of the concentration of impurities present in the plating solution. Upon the rejuvenation of the contaminated plating solution, the level of impurities present in the deposits reduces considerably.

3.2.2 Determination of Mechanical Properties

Hardness measurement is used to characterize the mechanical strength of the deposits produced. One of the major reasons for the use of chromium plating is due to its high mechanical strength. The most commonly used method for measuring hardness is the Rockwell tester. Carefully prepared deposits were used for this study. The data show that the sample prepared from the most contaminated solution (Set 1) has the lowest hardness value of 57.1 while the chromium deposited from a freshly prepared solution has the highest hardness value of 77.5.

When the Set 1 solution was purified and the deposit was produced, the hardness value of the deposit was found to be 69.6 - which represents an increase of 22%. The deposit produced from the less contaminated solution (Set 2) has a hardness value of 68.2. Upon purification of the solution and subsequent deposition, the hardness value increased to 77.5 (an increase of 14%) which is the same value that was obtained for the deposit produced from the freshly produced hard chromium plating solution.

Table 5. Rockwell Hardness Measurements

Sample	Hardness Value (mean/median)
1. Deposit from freshly prepared hard chromium solution (control)	77.5 / 77.0
2. Set 1 a) Deposit from spent solution b) Deposit from rejuvenated solution	57.1 / 58.0 69.6 / 69.0
3. Set 2 a) Deposit from spent solution b) Deposit from rejuvenated solution	68.2 / 68.0 77.5 / 78.0

3.2.3 Corrosion Resistance Properties

Electrochemical methods are employed to measure the corrosion resistance of metals and alloys. The method used in this study is called the DC potentiodynamic polarization method and this method is in accordance with the American Society of Testing Materials (ASTM) procedure, Number D-1242. The rate of corrosion of selected chromium coatings was determined in a chloride solution (33 g/l of distilled water). The procedure involved generation of current (i.e. metal dissolution rate) vs. potential (i.e. oxidizing power) diagram. The active-passive regions of chromium corrosion were determined. The net anodic and cathodic currents were calculated from the experimental data. The potential at which the anodic and cathodic currents equal one another is called the corrosion potential, E_{corr} and the current is named corrosion current, I_{corr}. The method used for calculation of corrosion characteristics is called the Tafel analysis. The corrosion rate in mils per year (MPY) is calculated using the Faraday law:

$$corrosion \quad rate = \frac{dW}{dt} = \frac{M\, I_{corr}}{nF} \tag{6}$$

where:

W = weight loss of specimen

M = atomic weight

n = valence of disollution

t = time,

F = Faraday constant

d = differential

The corrosion characteristics of the deposits produced are reported in Table 6. The deposit produced from a freshly prepared hard chromium solution showed the lowest metal dissolution rate. The rate of dissolution is found to be proportional to the amount of impurities present in the plating solutions. For example, the deposit produced from Set 1 solution which contains the highest level of metal impurities, is observed to have the highest corrosion (i.e. dissolution) rate. Once the contaminated solutions have been rejuvenated, the deposits produced exhibit greatly lowered metal dissolution rates. There rates are of nearly the same order of magnitude as the corrosion rate observed for the deposit produced from the freshly produced hard chromium plating solution.

Table 6. Corrosion Characteristics of Deposits

Sample	E_{corr}, mV	I_{corr}	Dissolution rate, MPY*
1. Deposit produced from freshly prepared hard chromium solution (control)	-100	0.27	0.04
2. Set 1 a) Deposit from spent solution b) Deposit from rejuvenated solution	 -945 -50	 1707 0.63	 265 0.10
3. Set 2 a) Deposit from spent solution b) Deposit from rejuvenated solution	 -265 -100	 316 0.63	 49.04 0.10

*Mils (one-thousand of an inch) per year.

3.2.4 Microstructural

A micrograph of deposits prepared from a freshly prepared hard chromium plating solution is shown in Figure 7. A magnification factor of 1000 was used. The micrograph shows some macro-cracks which are typical of chromium plating. The grains are observed to be relatively uniform and appear to form a continuous layer. Figures 8-a and 9-a are the micrographs of deposits produced from set 1 and set 2 solutions whereas Figures 8-b and 9-b are the micrographs of deposits produced from purified set 1 and set 2 solutions respectively. In comparison with the micrograph obtained for hard chromium deposit (Figure 7), micrographs of the deposits produced from the as-received set 1 and set 2 solutions appear to have grains whose boundaries do not touch one another and give

the appearance of being 'burnt' deposits. However, when the set 1 and set 2 solutions were purified by the application of electrical fields and then deposits were produced the micrographs show that the plating obtained has characteristics (see Figure 8-b and 9-b) which are very similar to that of the deposits produced from freshly prepared hard chromium plating solution (Figure 7).

3.3 Kinetics of Impurity Removal

3.3.1 Model Development

The following assumptions are implied in the development of the mathematical model presented below:

i) the movement of impurities from the anode compartment to the cathode is governed by:

   a) electromigration due to the opposite charges present on metal ions and the cathode;

   b) diffusion due to concentration gradients; and

   c) convection caused by the stirring of the solution;

ii) the pH of the solution does not change over the course of the reaction and hence no metal precipitation or sludge formation occurs;

iii) metal deposition at the cathode;

iv) insignificant resistance offered to the movement of ions by the porous membrane;

v) unidirectional movement of ions; and

vi) Initially the impurities are present in the anode compartment only.

The approach presented below involves performing mass balances over individual ionic species in the anode and cathode compartments whose movement is caused by the application of constant voltage across the anode and cathode.

The flux of ions of species i is given by (13):

$$J_i = -D_i \frac{\partial c_i}{\partial x} - u_i c_i \frac{\partial \phi}{\partial x} + c_i v(x) \tag{7}$$

where the first, second and third term respectively represent flux due to diffusion gradient, electromigration and convection. In equation [7], D is the diffusion coefficient, C is the concentration, x is the separation distance, ϕ is the potential and v is the velocity causing the convection. The mobility, u_i of species i is given by:

$$u_i = \frac{|z_i F D_i|}{RT} \tag{7-a}$$

where, z is the charge on the ion, F is the Faraday constant, R is the universal gas constant and T is the temperature in K.

Material Balance (Species) Over Anode Compartment

The decrease in the mass of the migrating species i equals its flux multiplied by the surface area A_p of the diaphragm, hence, using equation (7), we obtain:

$$\frac{dc_{ia}}{dt} = \left[- D_i \frac{\partial c_{ia}}{\partial x} - u_{ia} c_{ia} \frac{\partial \phi}{\partial x} + c_{ia} v(x) \right] \left(\frac{A_p}{V_a} \right) \tag{8}$$

where V_a is the volume of the anode compartment. The diffusion and convection terms are represented by an aggregate term that contains the mass transfer coefficient, k_{ma}, hence the above equation can be rewritten as:

$$\frac{dc_{ia}}{dt} = \left[-k_{ma}\left(c_{ia} - c_{ic}\right) - u_{ia} c_{ia} \frac{\partial \phi}{\partial x} \right] \left(\frac{A_p}{V_a} \right) \tag{9}$$

The above equation is simplified as shown below:

$$\frac{dc_{ia}}{dt} + \alpha_1 c_{ia} = \alpha_2 c_{ic} \tag{10}$$

where, $\alpha_1 = \left[k_{ma} + u_{ia} \frac{\partial \phi}{\partial x} \right] \sigma_1$ (10-a)

$$\alpha_2 = k_{ma} \sigma_1 \tag{10-b}$$

and

$$\sigma_1 = \frac{A_p}{V_a} \tag{10-c}$$

Material Balance (Individual Species) Over Cathode Compartment

The net change in the mass of the cation migrating to the cathode equals its rate of transport minus the rate of electrodeposition.

$$\frac{dc_{ic}}{dt} = \left[-D_i \frac{\partial c_{ic}}{\partial x} - u_{ic} c_{ic} \frac{\partial \phi}{\partial x} + c_{ic} v(x) \right] \left(\frac{A_p}{V_c} \right) - k_c \frac{A_c}{V_c} c_{ic} \tag{11}$$

The second term on the right hand side represents the amount electrodeposited. The rate constant, k_c, is a function of the electrode potential as determined by the Butler-Volmer equation. The diffusion and convection terms are represented again by an aggregate term that contains the mass transport coefficient, K_{ma}, hence we have:

$$\frac{dc_{ic}}{dt} = \left[-k_{ma}\left(c_{ia} - c_{ic}\right) - u_{ia} c_{ic} \frac{\partial \phi}{\partial x} \right] \left(\frac{A_p}{V_c} \right) - k_c \frac{A_c}{V_c} c_{ic} \tag{12}$$

The above expression can be rewritten as:

$$\frac{dc_{ic}}{dt} + \alpha_3 c_{ic} = \alpha_4 c_{ia} \tag{13}$$

where $\sigma_2 = \frac{A_c}{V_c}$ (13-a)

$$\sigma_3 = \frac{A_p}{V_c} \tag{13-b}$$

$$\alpha_3 = k_c \sigma_2 + k_{ma} \sigma_3 \tag{13-c}$$

and,

$$\alpha_4 = \left(k_{ma} + u_{ia} \frac{\partial \phi}{\partial x} \right) \sigma_3 = \alpha_1 (\sigma_3 / \sigma_1) \tag{13-d}$$

The two coupled first-order differential equations (10) and (13) are solved using the initial conditions: t = 0: $c_{ia} = c_{io}$, and $c_{ic} = 0$.

The solution to the differential equations is given by the following expression: [See Appendix I]

$$c_{ic} = \frac{\alpha_2 c_{io}}{(m_1 - m_2)} \left[e^{m_1 t} - e^{m_2 t} \right] \tag{14}$$

and

$$c_{ia} = \frac{c_{io}}{(m_1 - m_2)} \left[(m_1 + \alpha_1) e^{m_1 t} - (m_2 + \alpha_1) e^{m_2 t} \right] \tag{15}$$

where the exponents m_1 and m_2 are given by:

$$m_1, m_2 = \frac{-(\alpha_1 + \alpha_3) \pm \sqrt{(\alpha_1 - \alpha_3)^2 + 4\alpha_2 \alpha_4}}{2} \tag{16}$$

Thus, equations (14) and (15) describe the dynamic concentrations of individual ions in the cathode and anode compartments.

3.3.2 Kinetic Data and Model Validation

The metal concentration vs. time plots for both anolyte and catholyte are given in Figures 10-12. In these experiments o-phosphoric acids were used. As expected, the anolyte ion concentration is observed to initially decrease sharply with time and then the rate decreases asymptotically. The catholyte ion concentration, on the other hand, increased initially and reached a maximum and then decreased with time. The initial increase in concentration of metallic ions in the catholyte is due to the movement of ions to the cathode due to electromigration and concentration gradients. However, upon a sufficient build-up of concentration, the metal deposition ensues which results in a decrease in the catholyte metal concentration. This behavior is more pronounced in the case of nickel and copper migration to the cathode compartment as seen from Figures 11 and 12. The data on the experimental parameters and the amount of metal removal are presented in Tables 7 and 8. For example, 36.4% and 29% decrease in iron and nickel removal was observed in 24.4 and 25.4 hours, respectively. Up to 32% copper removal was observed in 7 hours. The rate of copper removal was found to be 300% times as great as the rate of nickel removal while the rate of iron removal was found to be 30% greater than the rate of nickel removal under similar experimental conditions.

Table 7: Experimental conditions for the validation of the kinetic model for removal of impurities.

Parameter	Iron	Nickel	Copper		
	Voltage, V				
	6.0	6.0	3.0	5.5	6.51
A_{pa} (dm^2)	5.02	4.95	5.50	4.83	4.77
V_a (dm^3)	1.95	1.94	1.79	1.91	1.89
V (volts)	5.00	6.50	3.00	5.50	6.51
x (cm)	4.00	4.00	4.00	4.00	4.00
A_{pc} (dm^2)	4.32	4.26	4.73	4.15	4.10
A_c (dm^2)	0.07	0.07	0.07	0.07	0.07
V_c (dm^3)	0.74	0.76	0.69	0.75	0.74
σ_1 (m^{-1})	25.70	25.55	30.72	25.27	25.26
σ_2 (m^{-1})	0.950	0.950	0.901	0.895	0.895
σ_3 (m^{-1})	58.46	56.18	68.12	55.32	55.27

Table 8: Metal Ion Removal

Experiments were carried out using applied cell voltage of 6.0 V. Other experimental conditions as in Table 1.

	Iron	Nickel	Copper
Initial concentration, mg/l	1,604	1,560	1,360
Final concentration, mg/l	1,020	1,108	924
Length of Experiment, h	24.4	25.4	7.0
% decrease in concentration	36.4	29.0	32
% decrease in concentration per unit time, h^{-1}	1.49	1.14	4.57

The equations developed in this model (Equations 12 and 13) were used to predict the concentration vs. time data. Using the experimental data, the mass transfer coefficient (k_{ma}), the heterogeneous rate constant (k_c), the mobility (u_i) and the diffusivity (D_i) were calculated (Table 9). The constants evaluated from the experimental data using the model developed are in general agreement with the experimental values published in the literature (13-15). The comparison between the predicted and published data (14) for the ionic mobility and diffusivity for nickel, iron and copper are provided in Table 10. An excellent agreement between the two values are observed for nickel and copper. However, in the case of iron, the model predicts slightly larger values for mobility and diffusivity. The reason for this observation may be due to the chromic acid - iron system used in this study. A good correlation between the experimental data and the predicted concentration vs. time data for the movement of three ions of iron, nickel and copper is obtained (Figures 10-12). The model fit assumes that nickel and copper electrode position begins 3 and 2 hours after the beginning of the experiments, respectively. The iron deposition was estimated to occur since the start of the experiment. The data obtained at various applied voltages for copper electromigration was further evaluated according to the following analysis. The flux near the surface of the cathode can be approximated by: $k_c(c_{ic} - 0) = k_c c_{ic}$, since the metal deposition at the cathode can be neglected. In addition, the potential gradient, $\frac{\partial \phi}{\partial x}$ can be approximated as E/δ, where E is the potential at the cathode and δ is the diffusion layer thickness at the cathode. Similarly $\frac{\partial C_i}{\partial x}$ can be approximated by $\frac{C_{ic}}{\delta}$. Substitution of these approximate values into equation (7) allows us the determination of E according to the following expression:

$$E = -\left(\frac{K_c\delta + D_i}{\mu_i}\right) \tag{17}$$

Assuming δ to be 20 μm, the cathodic potentials for copper deposition for a 2-electron transfer process are calculated (Table 11). Using the Butler-Volmer expression for copper deposition, the standard heterogeneous rate constant (k_0), the symmetry factor (α), and the number of electrons transferred (n) are calculated and reported in Table 11. The r^2 value for the regression fitting was greater than 0.98. In addition, the data show that the calculated values are in good agreement with the data known as kinetics of copper electrodeposition (15). This analysis further validates the model developed in this study.

Damjanovic, Setty and Bockris (15) have studied the mechanism and kinetics of electrocrystallization of copper on copper.

Table 9. Estimated physical parameters for the removal of metallic impurities

	Nickel	Iron	Copper		
	Cell Voltage, V				
	6.0	6.0	3.0	5.5	6.51
k_{ma} (m/hr)	$8.48 * 10^{-4}$	$28.79 * 10^{-4}$	$3.26 * 10^{-4}$	$5.39 * 10^{-4}$	$3.96 * 10^{-4}$
k_c (m/hr)	$2.19 * 10^{-2}$	$1.16 * 10^{-2}$	$1.01 * 10^{-2}$	$9.26 * 10^{-2}$	$10.17 * 10^{-2}$
U_i (m^2/V-hr)	$2.17 * 10^{-5}$	$15.9 * 10^{-5}$	$7.22 * 10^{-5}$	$4.77 * 10^{-5}$	$4.05 * 10^{-5}$
D_i (m^2/s)	$0.84 * 10^{-10}$	$6.09 * 10^{-10}$	$2.75 * 10^{-10}$	$1.85 * 10^{-10}$	$1.32 * 10^{-10}$

Table 10. Comparison of model predicted with published data.

	Published		Model Predicted	
	D_i	u_i	D_i	u_i
Nickel	$0.88*10^{-10}$	$7.09 * 10^{-5}$	$0.84 * 10^{-10}$	$2.17 * 10^{-5}$
Iron	$0.96 * 10^{-10}$	$5.04 * 10^{-5}$	$6.09 * 10^{-10}$	$15.9 * 10^{-5}$
Copper	$0.95 * 10^{-10}$	$6.70 * 10^{-5}$	$1.32 * 10^{-10}$	$7.22 * 10^{-5}$

Table 11: Estimated Parameters of the Butler Volmer Equation for Copper Deposition

Parameter	
δ (μm)	20
αn	1.496
k_0 (m/hr)	$4.35 * 10^{-3}$
$\alpha_{(n=2)}$	0.748
r^2	0.98

They derived the following approximate expression for the rate of growth (P) of the deposits as a function of the current density (I):

$$P = 3.75I \qquad (12).$$

For the current density (16.87 mA/cm^2) used in this study, the rate of growth is calculated to be 63.3 A/s. It was observed by Damjanovic et. al. (15) that the actual rate of a macrostep propagation is about 7 times larger than the calculated value. This implies that the rate of propagation of a macrostep is about 442.8 A/s.

Since the surface of the deposit produced is not smooth but of the shape of a pyramid, the expression for the growth rate is rewritten in the following form:

$$growth\ rate = P_0 + 3.75I \cot \gamma$$

where γ is the inclination of the pyramidical surface of the deposit with the substrate. The value for P_0 observed by Damjanovic (15) is 55 A/s where as the angle γ from our deposits is around 0.5^0. According to the above equation, the rate of growth is 7304 A/s or approximately 0.0026 m/hr. The observed rate from our experiments is 0.004 m/hr. Based upon the above analysis, it appears that since the theoretical rate of growth and observed rate of growth are of the same order of magnitude, the model developed in the paper appears to be valid.

One of the important assumptions of this model is that the cathode pH does not vary greatly so as to cause metal precipitation or sludge formation. Figure 13 is a plot of the catholyte pH vs. time. The data show that for the duration of the experiment, the solution pH did not change significantly enough to cause metal precipitation. In the case of nickel and copper removal, the solution pH did increase somewhat. We ascribe this change to the evolution of hydrogen gas at the cathode. The hydrogen ions could electromigrate from the anode to the cathode, and thus offset the increase in the catholyte pH, as seems to be the case for pH vs. time behavior during iron removal.

3.4 Regeneration of Hexavalent Chromium

3.4.1 Model Development

In the analysis presented below, the two ionic species of chromium, i.e. trivalent chromium Cr^{3+} and dichromate anion $Cr_xO_y^{2-}$ are considered. For the sake of simplicity, we will consider that complete chromium reduction $Cr^{6+} \rightarrow Cr^0$ involves only dichromate ions and disregard higher polychromates. The movement of ions is assumed to be governed by concentration gradients and electromigration according to the flux equation (7). The diffusion and convection terms in equation (7) are lumped together by an aggregate term that is characterized by the mass transfer coefficient, K_{mi}, and therefore, the flux equation can be rewritten as:

$$J_i = K_{mi}\Delta x_i - u_i x_i\left(\frac{\partial \phi}{\partial z}\right) \qquad (19)$$

The development of the following mathematical model includes performing mass balances on the two chromium species for each of the two compartments of the electrochemical cell. The anode and cathode concentrations are represented by letters x and y respectively, and subscripts *1* and *2* represent Cr^{3+} and $\underline{Cr_xO_y}^{2-}$, respectively. Implicit in the model is the assumption that the resistance offered to the transfer of ionic species by the porous membrane is negligible. It is also hypothesized that the electrode potential at the anode and cathode remain constant over the course of experiments and hence, the rate constants for various electrochemical reactions listed below can be assumed to remain invariant.

$$Cr^{3+} \xrightarrow{K_{01}} Cr^{6+} \quad \left[as\ Cr_xO_y{}^{2-}\right] \qquad \text{(anode)}$$

$$Cr^{6+} \xrightarrow{K_{02}} Cr^{3+} \qquad \text{(cathode)}$$

$$Cr^{6+} \xrightarrow{K_{03}} Cr^{0} \qquad \text{(cathode)}$$

A. Cr^{3+} Balance

The schematic block-diagram for the movement of trivalent chromium ions is presented in sketch below.

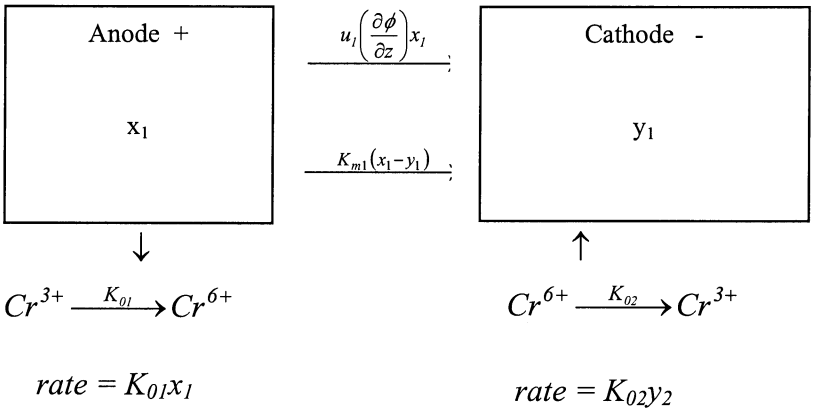

Anode:

`The mass balance for trivalent chromium ions in the anodic chamber can be written as:

$$0 - K_{01}x_1A_a = u_1\left(\frac{\partial \phi}{\partial z}\right)x_1A_p + K_{m1}(x_1 - y_1)A_p + V_a\frac{\Delta x_1}{\Delta t}$$

On rewriting the above expression, it assumes the form presented below:

$$\frac{dx_1}{dt} = -a_1x_1 + b_1y_1 \qquad (20)$$

The constants, a_1 and b_1, are listed in Table 12.

Cathode:

Similarly for the cathode chamber, the mass balance expression for trivalent chromium is given by:

$$u_1\left(\frac{\partial \phi}{\partial z}\right)x_1A_p + K_{m1}(x_1 - y_1)A_p + K_{02}y_2A_c = V_c\frac{\Delta y_1}{\Delta t}$$

which can be rewritten as:

$$\frac{dy_1}{dt} = a_1^1x_1 - b_1^1y_1 + c_1^1y_2 \qquad (21)$$

The constants, $a_1^{'}$, $b_1^{'}$ *and* $c_1^{'}$, are listed in Table 12.

B. $\underline{Cr_xO_y^{2-}\ \text{Balance}}$

The following sketch shows the fate of $Cr_xO_y^{2-}$ anion during the process.

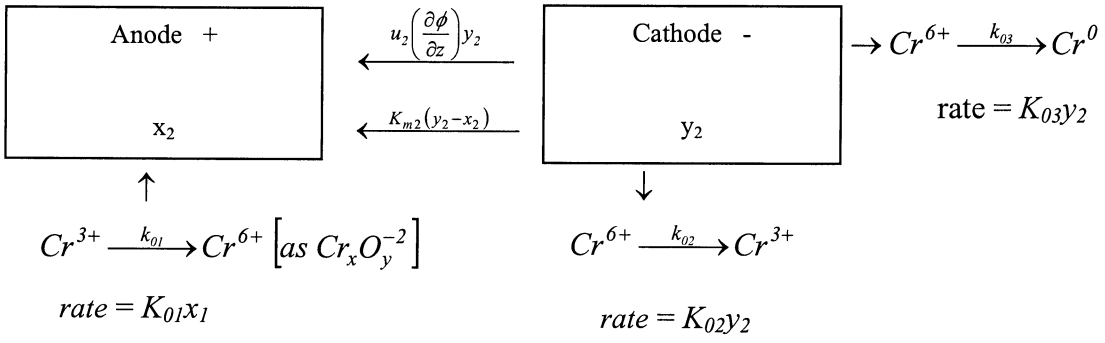

For the trivalent chromium species, the differential mass balances on the chromium anion for anode and cathode compartments are given by the following equations:

$$\frac{dx_2}{dt} = a_2x_1 - b_2x_2 + c_2y_2 \qquad (22)$$

$$\frac{dy_2}{dt} = a_2^1x_2 - b_2^1y_2 \qquad (23)$$

Coefficients of the equations (20) - (23) are listed in Table 12. The four coupled equations (Eqs. 20-23) are solved by an elimination of variables method outlined in Appendix II. The solution for concentration x_1, x_2, y_1 and y_2 involves estimation of exponential terms as listed in Appendix II.

Table 12 Coefficients for equations (4-7)

$$a_1 = K_{01}\sigma_3 + \left[K_{m1} + u_1\left(\frac{\partial\phi}{\partial z}\right)\right]\sigma_1$$

$$b_1 = K_{m1}\sigma_1$$

$$a_1^1 = \left[K_{m1} + u_1\left(\frac{\partial\phi}{\partial z}\right)\right]\sigma_2$$

$$b_1^1 = b_1\left(\frac{\sigma_2}{\sigma_1}\right)$$

$$c_1^1 = K_{02}\sigma_4$$

$$a_2 = K_{01}\sigma_3$$

$$b_2 = K_{m2}\sigma_1$$

$$c_2 = \left[K_{m2} + u_2\left(\frac{\partial\phi}{\partial z}\right)\right]\sigma_1$$

$$a_2^1 = b_2\left(\frac{\sigma_2}{\sigma_1}\right)$$

$$b_2^1 = (K_{02} + K_{03})\sigma_4 + u_2\left(\frac{\partial\phi}{\partial z}\right)\sigma_2 + K_{m2}\sigma_2$$

$$\sigma_1 = A_p / V_a$$

$$\sigma_2 = A_p / V_c$$

$$\sigma_3 = A_a / V_a$$

$$\sigma_4 = A_c / V_c$$

3.4.2 Kinetic Studies and Model Validation

A total of 4 figures (Fig. 14-17) represent the data on hexavalent chromium and trivalent chromium concentration vs. time from four experiments. The initial hexavalent chromium concentration in these four experiments was kept at 29, 98, 108, and 127 g/l, while the total chromium concentration in all the experiments (except for the experiment in which initial hexavalent chromium concentration of 29 g/l was used) was maintained at 130 g/l (corresponding to 250 g/l of CrO_3). Bi-doped lead dioxide on PbO_2 coated lead substrate was used as anode for these experiments. A more dilute solution (43 g/l of total chromium) was used for the experiment that involved initial hexavalent chromium concentration of 29 g/l. Both Bi-doped lead dioxide on PbO_2 coated lead substrate and anodized lead were used for regeneration via reoxidation of hexavalent chromium. The amount of trivalent chromium was adjusted to maintain the total chromium concentration. 2.5 g/l of sulfate, which acts as a catalyst for chromium deposition, was added. A constant voltage of 5 V was applied across the electrochemical cell which was maintained at a temperature of 45 ^{o}C. The data show that for the experiment using low initial concentration of chromium, the concentration of regenerated hexavalent chromium increases rather rapidly in the anode compartment. As an example, the hexavalent chromium concentration increases by about 218% in about 23 hours (Figure 14) when the initial hexavalent chromium concentration in the solution is 29 g/l. The trivalent chromium concentration decreases with time and reduces to a negligible amount at the end of the experiment. As expected, the hexavalent chromium concentration in the cathode compartment decreases with time due to its migration to the anode as well as by reductions to trivalent chromium and to the metallic chromium at the cathode. When an

initial chromium (Cr^{6+}) concentration of 98 g/l was used, the data show that its concentration initially increases with time in the anode compartment, reaches a maximum of about 120 g/l and then declines somewhat with further increase in time. The initial increase in concentration is attributed to electromigration of hexavalent chromium from the cathode to the anode as well as electrocatalytic anodic oxidation of trivalent chromium to hexavalent chromium. However, when the hexavalent chromium concentration in the anode compartment is significantly greater that that in the cathode compartment, mass transfer rate of the hexavalent chromium from the anode to the cathode compartment (back diffusion) becomes significant in comparison to its rate of electromigration from the cathode to the anode. In addition, the rate of hexavalent chromium regeneration decreases with time due to a decrease in the trivalent chromium concentration in the anode compartment. The increase in hexavalent chromium concentration for relatively large initial concentrations of hexavalent chromium (Figure 16 and 17) was relatively modest. Nonetheless, the maximum chromium concentration of 130-135 g/l is achievable. In order to compare the effect of various anode materials on the increase in hexavalent chromium concentration, one experiment using lead dioxide as anode (at the lowest Cr^{6+} initial concentration of 29 g/l) was carried out. The data in Figure 18 show that Bi-doped PbO_2 is much more effective to its PbO_2 counterpart in that the hexavalent chromium concentration increases much more rapidly with time due to its use. Whereas the use of PbO_2 coated lead anode results in only 67 % increase, the Bi-doped PbO_2 results in about 218 % increase in hexavalent chromium concentration under identical experimental conditions.

The experimental data shown in Figure 14-18 were fit to the mathematical model developed in this paper (Appendix II). The constants described in the model were estimated using the Levenberg-Marquadt algorithm for non-linear parameter estimation [16]. The objective function was to minimize the total errors between experimental and predicted values for each species after normalization with the measurement error under the constraint that the errors for individual species were also minimized. The values of constants of integration, C_i's, were determined analytically by solving for the initial conditions, once the remaining constants were determined. The results of the parameter estimation and the comparison of the experimental values versus predicted values are provided in the following paragraphs. . The results are shown in Tables 13, 14 and 15.

The results presented for Table 13 corresponds closely to that found in literature [14]. For example, the mobility of trivalent chromium was found to be 30.2 $*10^{-5}$ m^2/V-hr, while that reported in literature is that of 20.5 * 10^{-5} m^2/V-hr. The estimated values of the mass transfer coefficients show that the complex chromate anions have a greater mobility as compared to that of the trivalent chromium cation. Table 14 shows that all the exponents ($m_i's$) of the terms describing various concentrations in the mathematical model are negative. Thus, the rates of change in concentration decreases with time and may eventually change the direction of change. This is reflected in the fact that the concentration of hexavalent chromium in the anode chamber decreases while that in the cathode chamber increases after around 20 hours of running the experiments. The anodic and cathodic potentials were monitored as a function of time. The data shown in Figure 19 reflect that the assumption made in the mathematical analysis, that the potentials are almost invariant with time is valid.

As seen in Table 13, the rate of oxidation of trivalent chromium to hexavalent chromium is found to be over 4 times greater in the case of the Bi-doped anode than that of the simple commercial PbO_2 coated lead electrode for the same applied voltage and same initial concentrations and is reflected in the concentration of hexavalent chromium in the anode chamber as seen in Figure 18. The reason for this improvement can be explained through the following mechanism that was provided by Hsiao and Johnson [17]. According to this mechanism the labile surface-bound oxygen atom is generated as an intermediate product of the hydrogen evolution. These oxygen atoms probably exist as adsorbed hydroxyl radicals. These oxygen atoms are then transferred to the products of the electrocatalyzed anodic reactions as shown in Eq [24]-[25], where $M[\ ]$ represents the unpopulated surface site, R is the reactant and RO is the product of one oxygen transfer reaction. The rate of concurrent evolution of oxygen (Eq [26]) is to be reduced for efficient O-transfer reactions.

$$M[\ ] + H_2O \rightarrow M[OH] + H^+ + e^- \quad (24)$$

$$M[OH] + R \rightarrow M[\ ] + RO + H^+ + e^- \quad (25)$$

$$M[OH] + H_2O \rightarrow O_2 + 3H^+ + 3e^- \quad (26)$$

In order to achieve this goal, a suitable electrode has to be found with high oxygen evolution overpotential such as lead or lead dioxide. When using doped lead dioxide electrodes, hydroxyl atoms are adsorbed on the doped (Bi) sites at an enhanced rate and are transferred to the lead sites for the O-transfer to take place. Thus, an ideal anode for enhanced O-transfer reactivity can be envisioned as an inert matrix having a large oxygen evolution overpotential into which is incorporated a low-density array of

catalytic sites characterized by low O_2 evolution overpotential. Owing to the low area of the sites, the background current for oxygen evolution would be minimal. However, a high flux of the diffusing reactant exists at the sites. If the inter-site distances were less than the diffusion layer thickness, highly efficient oxygen transfer reactions can be expected at the electrode.

Table 13. Estimated physical constants.

	Bi-doped PbO_2 anode	PbO_2 anode
k_{m1} (m/hr)	$27.1 * 10^{-5}$	$27.1 * 10^{-5}$
k_{m2} (m/hr)	$90.2 * 10^{-5}$	$90.2 * 10^{-5}$
k_{01} (m/hr)	$66.8 * 10^{-3}$	$15.8 * 10^{-3}$
k_{02} (m/hr)	$13.8 * 10^{-3}$	$13.8 * 10^{-3}$
u_1 (m^2/V-hr)	$30.2 * 10^{-5}$	$30.2 * 10^{-5}$
u_2 (m^2/V-hr)	$80.9 * 10^{-5}$	$80.9 * 10^{-5}$
k_{03} (m/hr)	$1.8 * 10^{-3}$	$1.8 * 10^{-3}$

Table 14. Estimated values for the exponents in Eq. B8, B10, B11, and B12.

	Bi-doped PbO_2 anode				PbO_2 anode
Initial Cr^{6+}	29 g/l	98.5 g/l	108 g/l	127 g/l	29 g/l
m_1	-0.1510	-0.0759	-0.1517	-0.1514	-0.0990
m_2	$-2*10^{-5}$	-0.1505	-0.0042	-0.0052	-0.0865
m_3	-0.0865	-0.1374	-0.0854	-0.0599	-0.0032
m_4	-0.1401	-0.0050	-0.1099	-0.0775	-0.1839

Table 15. Estimated values for the coefficients in Eq. B8, B10, B11, and B12.

	Bi-doped PbO_2 anode				PbO_2 anode
Initial Cr^{6+}	29 g/l	98.5 g/l	108 g/l	127 g/l	29 g/l
c_1	12.5921	-3.4420	32.3238	5.8767	2.9894
c_2	0.3487	37.3673	1.6628	2.5706	9.6771
c_3	-1.1487	-3.9532	-5.5645	0.7947	-0.6987
c_4	-0.2921	1.5378	1.8779	-6.1420	-0.4678

4. GUIDELINES FOR PRACTICAL OPERATIONS

Based upon our research and experience we suggest the following:

1. The cathode compartment should contain freshly prepared hard chromium plating solution as an electrolyte
2. A current density of 15.6 A/ft^2 or a cell voltage of 6-8 V is recommended.
3. After about 12-14 hrs of operations, the lead cathode should be removed and the deposits consisting of metals need to be removed. Thereafter, new freshly prepared catholyte ought to be used.
4. The catholyte, concentrated with metallic impurities could either be treated with an appropriate adsorbent to extract metals or its pH can be raised to precipitate the metals.
5. A note of caution. When the applied current (or voltage is turned off, the porous pot must be removed immediately from the tank so as to prevent any back diffusion of impurities from the solution in the cathode chamber to the plating solution.

5. CONCLUSIONS

The research has shown that application of voltage across the two electrodes placed in a solution containing metallic impurities results in the migration of metal cations in the cathode compartment. The impurities are concentrated in the catholyte and can be removed either by electrodeposition or precipitation (which is brought about by the increase in solution pH). Chromic acid appears to a suitable choice as a catholyte because it is readily available in chromium plating shops, it is inexpensive and offers very little solution resistance. Research has shown that trivalent chromium is effectively regenerated at Bi-doped lead dioxide anode. The properties of chromium deposits produced from the regenerated plating solutions are far superior to those obtained from contaminated plating solutions and are comparable to the properties of the deposits obtained from freshly produced hard chromium plating solutions. Although the mobility of ions is slow, nonetheless the approach described here for plating solution purification and regeneration is used in the industry over the weekends and during the night when the bath is not utilized for plating purposes. This purification process does not require any supervision.

NOMENCLATURE

A: area, cm^2

C: constant of integration

c: concentration, $moles/cm^3$

D: diffusivity, m^2/s

E: potential at the cathode, V

F: Faraday constant, 96485 coulombs/equiv

F: Faraday constnat, 96485 coulombs/equivalent

I: current density, A/cm^2, A/ft^2

J: flux, $moles/m^2$-s

K: heterogeneous rate constant, m/s

k_c: heterogeneous rate constant, m/s

k_m: mass transfer coefficient, m/s

n: ionic charge (integer)

P: growth rate, m/s

R: universal gas constant, 8.314 J/mol-K

t: time, s

T: temperature, K

u: ionic mobility, m^2/V-s

V: volume, m^3

x: separation distance, m

x: anodic concentration, $moles/m^3$

y: cathodic concentration, $moles/m^3$

z: charge

z: separation distance, cm

Greek letters

υ: velocity, m/s

ϕ: potential, V

δ: diffusion layer thickness, m

γ: inclination of the pyramid surface

Subscripts

1: Cr^{3+}

2: $Cr_xO_y^{2-}$

a: anode

c: cathode

m: mass transfer coefficient

i: species

p: porous pot

o: time = 0

01: oxidation of trivalent chromium

02: reduction to trivalent chromium

03: chromium deposition

REFERENCES

1. Chessin, H., and Knill, E.C., Plating and Surface Finishing 73, 8 (1986), 26.
2. Boyce, A.R., and Kavanaugh, D.J., Proceedings of 9th AESF/EPA Conference on Environmental Control in Metal Finishing Industries (1980).
3. Mandich, N. V., Li, C-C, and Selman, J.R., Practical and Theoretical Aspects of Regeneration of Chromic Acid Plating Solution, via Electrolytic Purification, *Plating And Surface Finishing,* 84, 12. (1997).
4. Guddari, M., Holsten, C., Li, C.-C., and Mandich, N.V., "The Use of Porous Ceramic Diagrapham for the Removal of Metallic Impurities from Chromium Plating Baths," *J. Appl. Electrochemistry*, accepted for publication.
5. Reid, F. H., and Goldie, W., *Gold Plating Technology,* Electrochemical Publications, Glasgow, U.K., 7 (1974).
6. Mandich, N. V., "Chemistry and Theory of Chromium Deposition – Part I," *Plating and Surface Finishing,* 81, 108-115 (1997).
7. Mandich, N.V., "Removal of Metallic Impurities from Plating Solutions by Electrocoagulation," AESF Chromium Colloqium, Orlando, FL (Jan. 1994).
8. Lalvani, S.B., Mandich, N.V., "Removal of Metallic Impurities in Chromium Plating Solutions by Electrocoagulation," Illinois Waste Management and Research Center, Champaign, IL, Project No. 97025, (1997).

9. Vora, R. J., Taylor, S. R., and Stoner, G. E., "Factors Affecting the Performance of PbO_2 Anodes in the Generation of Hexavalent Chromium" in F. Hine et al. (Eds), Proceedings of the Symposium on Performance of Electrodes for Industrial and Chemical Processes, The Electrochemical Society, (1989) 279-289.
10. Mayne, J. E. O., "Inhibition of Corrosion of iron and Aluminum", British Corrosion J. 31 (3), 232-234 (1996) .
11. Lalvani, S.B., Wiltowski, T., Weston, A., and Mandich, N.V., "Removal of Hexavalent Chromium and Metal Cations by a Novel Carbon Adsorbent," Carbon, 36, 7, 1219-1224 (1998).
12. Mandich, N.V., Lalvani, S.B., and Wiltowski, T., "Selective Removal of Chromate Anion by New Carbon Adsorbent," Metal Finishing, 96, 39-45, (1998).
13. Bard. A. J., and Faulkner, L. R., *Electrochemical Methods- Fundamentals and Applications*, John Willey and Sons, Inc.,, New York, USA (1980).
14. Guddati, S. L., Holsen, T. M., and Selman, J. R., "Optimization of Porous Ceramic Diaphragm Cell Operation for the Removal of Metallic Impurities from Chrome Plating Bath", *Report for Summer Research Grant Program*, AESF, Orlando, FL (1995)
15. Damjanovic, A., Setty, T. H. V., Bockris, J. O' M., " Effect of Crystal Plane on the Mechanism and Kinetics of Copper Crystallization", *J. Electrochemical Society,* 113, 5, 431-440 (1966)

16. Ratkowsky, David A., Nonlinear Regression Modeling, A Unified Practical Approach, Marcel Dekker, New York (1983).

17. Hsiao, Y-L. and Johnson, D. C., "Electrocatalysis of Anodic Oxygen Transfer Reactions: Chlorine Doped Lead Dioxide Electrodes", *J. Electrochemical Soc.*, 136 (12), (1989) 3704-3711.

APPENDIX I

Consider the two coupled first ordered differential equations:

$$\frac{dy}{dt} + \alpha_1 y = \alpha_2 x \qquad \text{(A1)}$$

$$\frac{dx}{dt} + \alpha_3 x = \alpha_4 y \qquad \text{(A2)}$$

from (A1): $x = \frac{1}{\alpha_2}\frac{dy}{dt} + \frac{\alpha_1}{\alpha_2} y$ (A1')

differentiate (A1) w.r.t. time, t:

$$\frac{d^2 y}{dt^2} + \alpha_1 \frac{dy}{dt} = \alpha_2 \frac{dx}{dt}$$

Substitute (A2) in the above equation

i.e. $\frac{d^2 y}{dt^2} + \alpha_1 \frac{dy}{dt} = \alpha_2 [\alpha_4 y - \alpha_3 x]$

Substitute (A1') in the above equation and rearrange the terms:

i.e. $\frac{d^2 y}{dt^2} + (\alpha_1 + \alpha_3)\frac{dy}{dt} + (\alpha_1 \alpha_3 - \alpha_2 \alpha_4) y = 0$

the solution to above second order differential equation is given by:

$$y = ae^{m_1 t} + be^{m_2 t} \qquad \text{(A3)}$$

where the exponents are given by

$$m_1, m_2 = \frac{-(\alpha_1 + \alpha_3) \pm \sqrt{(\alpha_1 - \alpha_3)^2 + 4\alpha_2 \alpha_4}}{2}$$

substitute (A3) into (A1'):

$$x = \frac{a(m_1 + \alpha_1)}{\alpha_2} e^{m_1 t} + \frac{b(m_2 + \alpha_1)}{\alpha_2} e^{m_2 t} \qquad \text{(A4)}$$

using the initial conditions, t = 0; y = 0 and x = c_{io}, we solve for constants a and b and their substitution equations (A3) and (A4) yields the following:

$$y = \frac{c_{io}\alpha_2}{(m_1 - m_2)}\left[e^{m_1 t} - e^{m_2 t}\right] \qquad \text{(A5)}$$

and

$$x = \frac{c_{io}}{(m_1 - m_2)}\left[(m_1 + \alpha_1)e^{m_1 t} - (m_2 + \alpha_1)e^{m_2 t}\right] \qquad \text{(A6)}$$

Appendix II

Consider the following coupled differential equations:

$$\frac{dx_1}{dt} = -a_1 x_1 + b_1 y_1 \tag{B1}$$

$$\frac{dy_1}{dt} = a_1^1 x_1 - b_1^1 y_1 + c_1^1 y_2 \tag{B2}$$

$$\frac{dx_2}{dt} = a_2 x_1 - b_2 x_2 + c_2 y_2 \tag{B3}$$

$$\frac{dy_2}{dt} = a_2^1 x_2 - b_2^1 y_2 \tag{B4}$$

From Eq. (B1):

$$y_1 = \frac{1}{b_1}\left[\frac{dx_1}{dt} + a_1 x_1\right] \tag{B1-a}$$

Substitution of Eq. (B1-a) into Eq. (B2) and solving for y_2 gives

$$y_2 = \frac{1}{b_1 c_1^1}\left[\frac{d^2 x_1}{dt^2} + q\frac{dx_1}{dt} - r x_1\right] \tag{B5}$$

where $q = a_1 + b_1^1$ (i)

$r = a_1^1 b_1 - a_1 b_1^1$ (ii)

Substitution of Eq. (B5) into Eq. (B4) and solving for x_2 gives:

$$x_2 = \frac{1}{a_2^1 b_1 c_1^1}\left[\frac{d^3 x_1}{dt^2} + p\frac{dx_1^2}{dt^2} - f\frac{dx_1}{dt} - g\, x_1\right] \tag{B6}$$

where $p = q + b_2^1$ (iii)

$f = r - q\, b_2^1$ (iv)

$$g = r\, b_2^1 \qquad \text{(v)}$$

Substitution of Eqs. (B5) and (B6) into Eq. (B3) and solving for x_1

$$\frac{d^4x_1}{dt^4} + (b_2 + p)\frac{d^3x_1}{dt^3} + (b_2 p - a_2^1 c_2 - f)\frac{d^2x_1}{dt^2} - (g + b_2 f + a_2^1 c_2 q)\frac{dx_1}{dt} - (b_2 g - a_2^1 c_2 r + a_2 a_2^1 b_1 c_1^{\,1})x_1 = 0 \qquad \text{(B7)}$$

Solution to the above fourth order differential equation is given by:

$$x_1 = \sum_{j=1}^{4} C_j e^{m_j t} \qquad \text{(B8)}$$

where C_j is the constant of integration and the four exponents, m_j are given by the roots of the algebraic expression:

$$D^4 + (b_2 + p)D^3 + (b_2 p - a_2^1 c_2 - f)D^2 - (g + b_2 f + a_2^1 c_2 q)D - (b_2 g - a_2^1 c_2 r + a_2 a_2^1 b_1 c_1^{\,1}) = 0 \qquad \text{(B9)}$$

Substitution of x_1 from equation (B8) into equations (B6), (B1-a) and (B5) yields the following expressions:

$$x_2 = \frac{1}{a_2^1 b_1 c_1^1} \sum_{j=1}^{4} (m_j^3 + p m_j^2 - f m_j - g) C_j e^{m_j t} \qquad \text{(B10)}$$

$$y_1 = \frac{1}{b_1} \sum_{j=1}^{4} (m_j + a_1) C_j e^{m_j t} \qquad \text{(B11)}$$

$$y_2 = \frac{1}{b_1 c_1^1} \sum_{j=1}^{4} (m_j^2 + q m_j - r) C_j e^{m_j t} \qquad \text{(B12)}$$

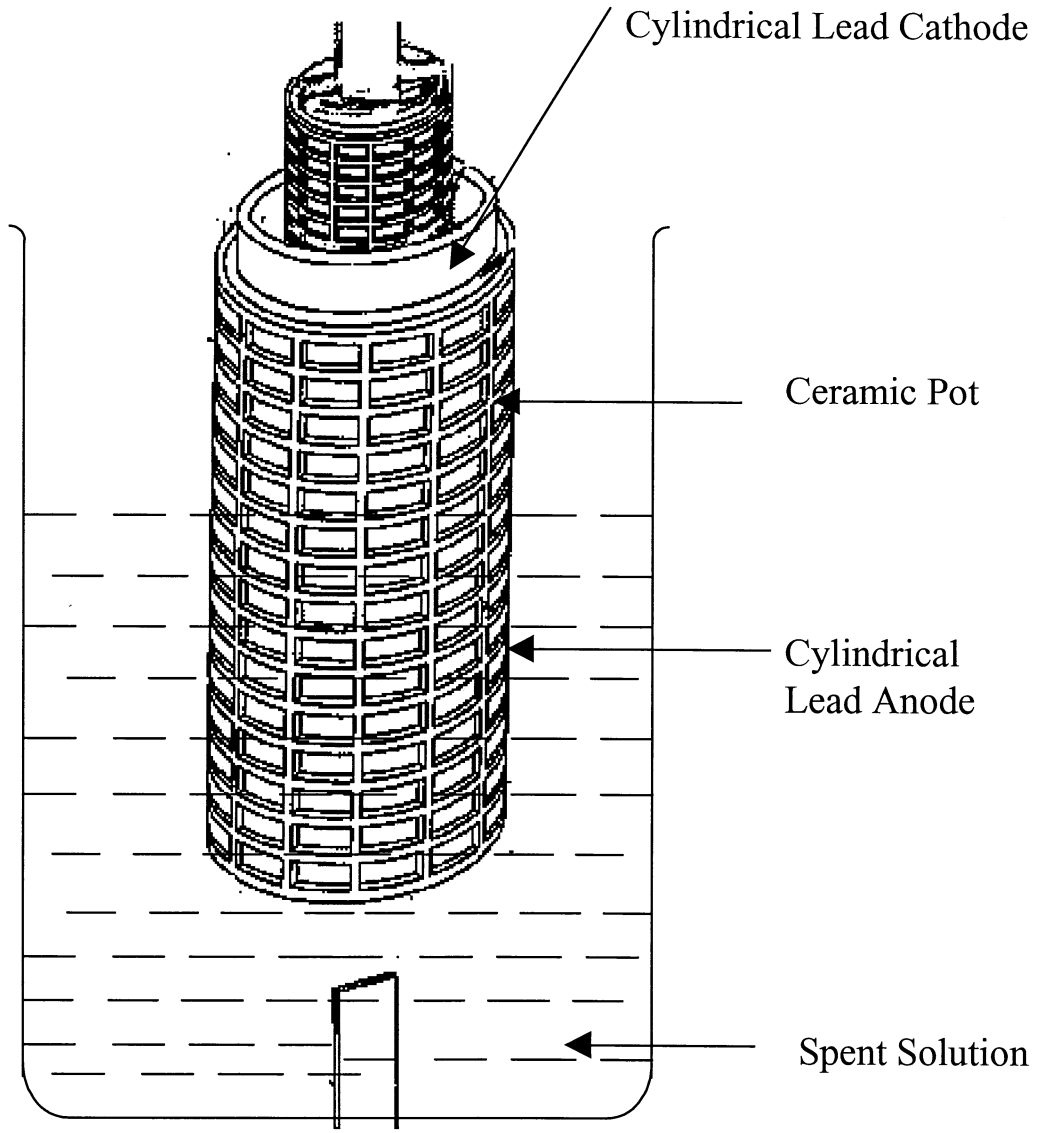

Figure 1 A Sketch of Electrochemical Reactor used in the Laboratory

Figure 2 in Main Manuscript

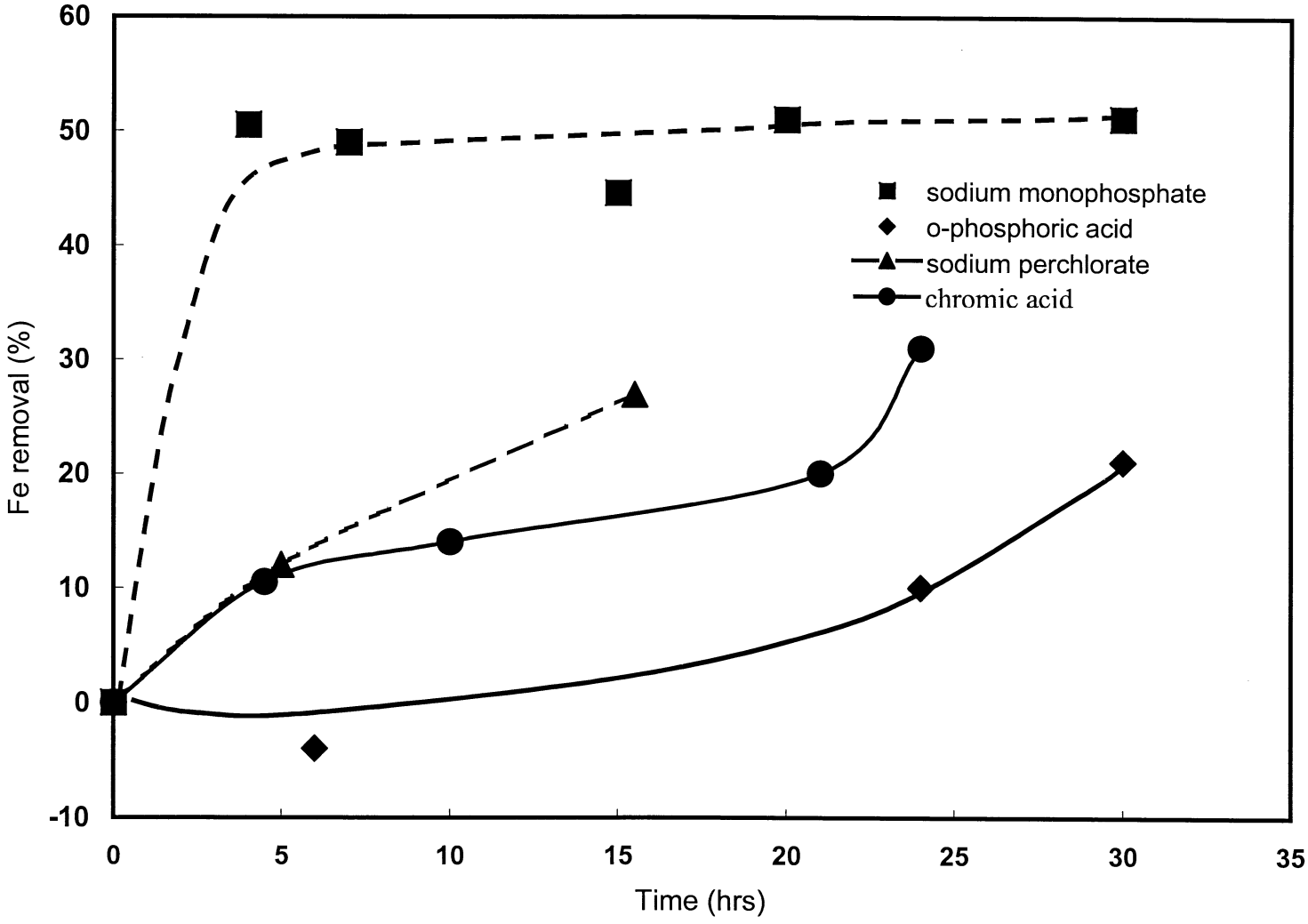

Figure 3. Iron Removal vs. Time

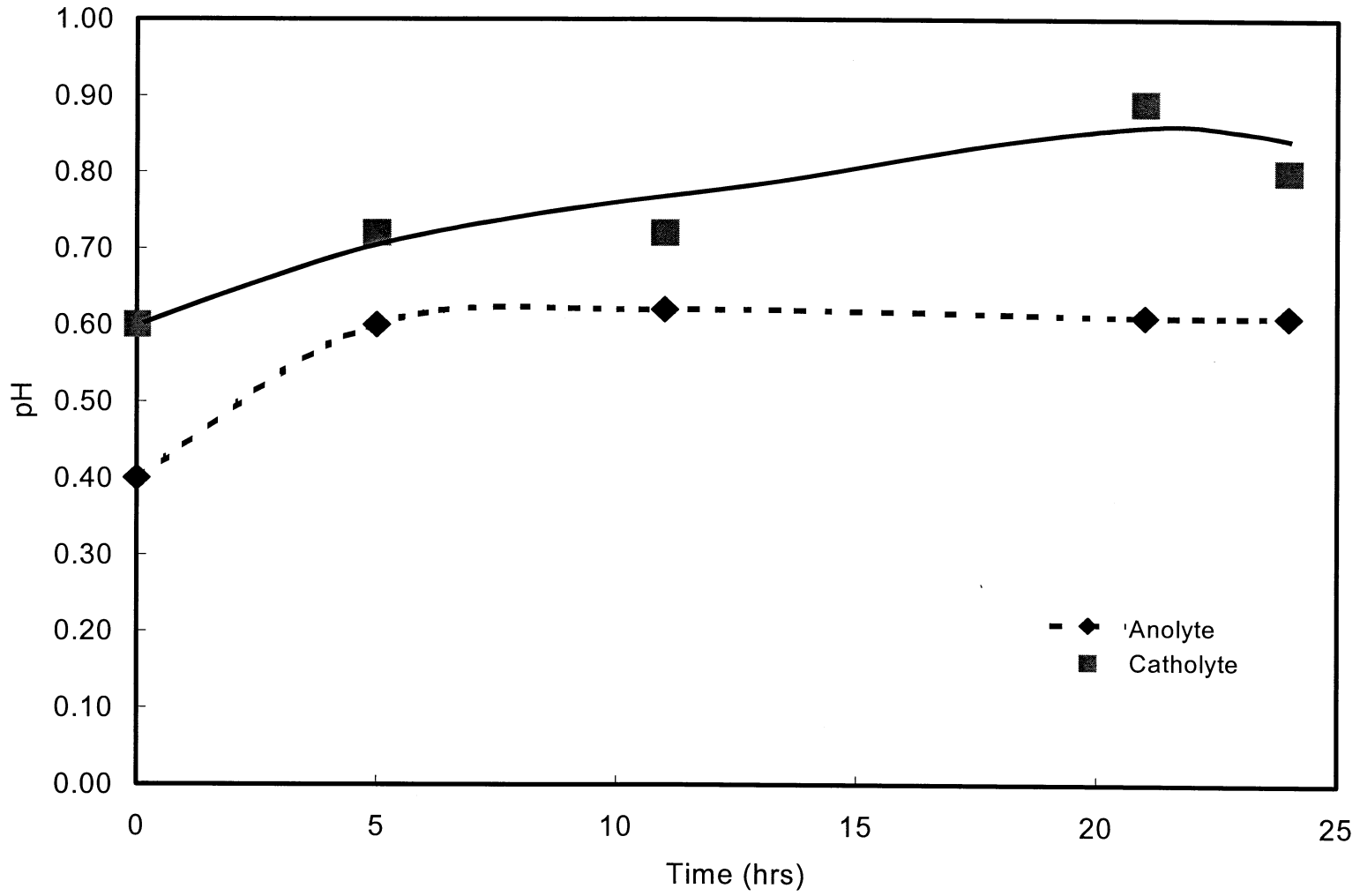

Figure 4 pH vs. Time

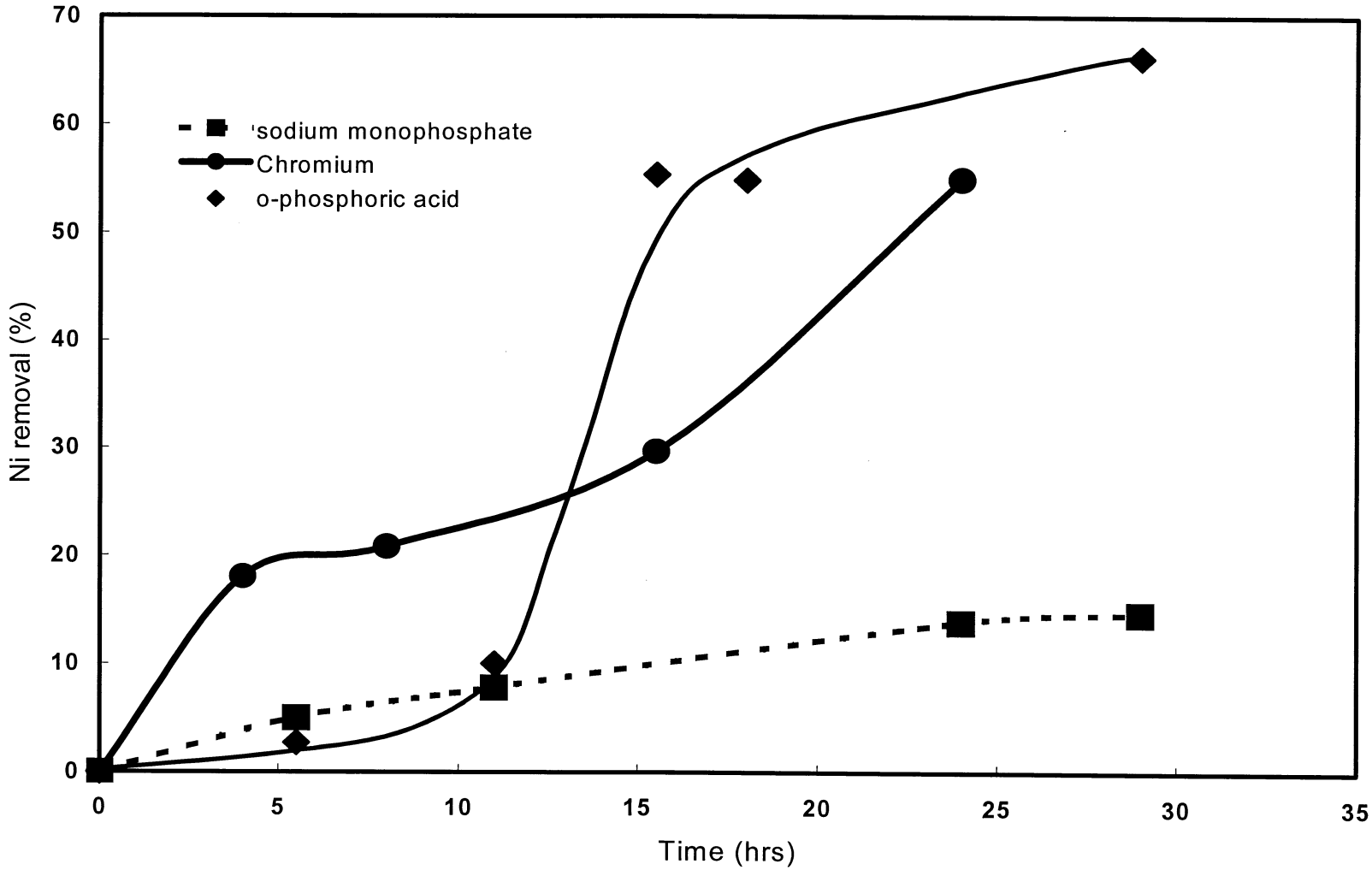

Figure 5. Nickel Removal vs. Time
Catholytes: O-phosphoric Acid and Sodium Monophosphate

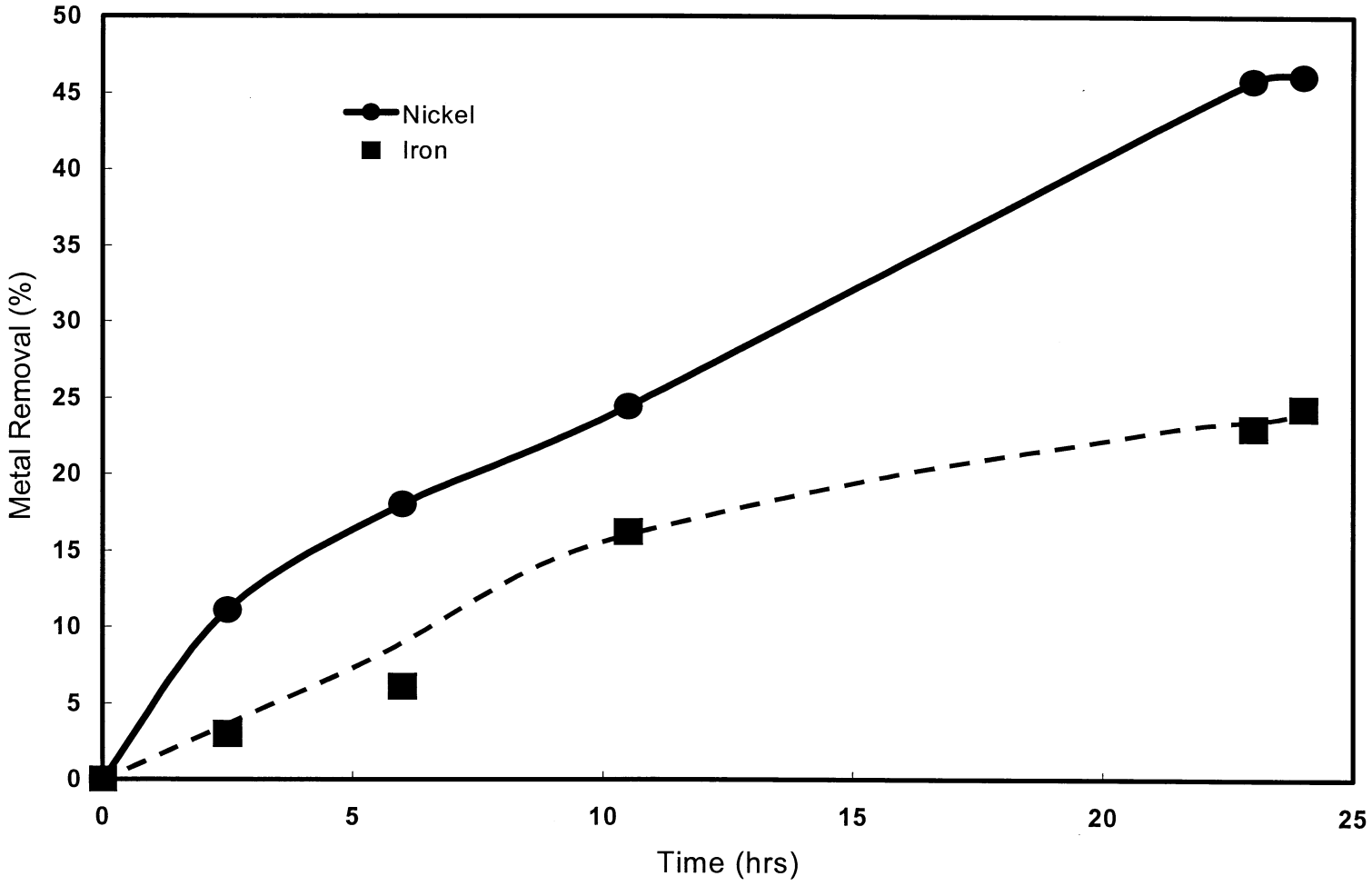

Figure 6. Nickel and Iron Removal vs. Time
Catholyte: Chromic Acid (2.5 M)

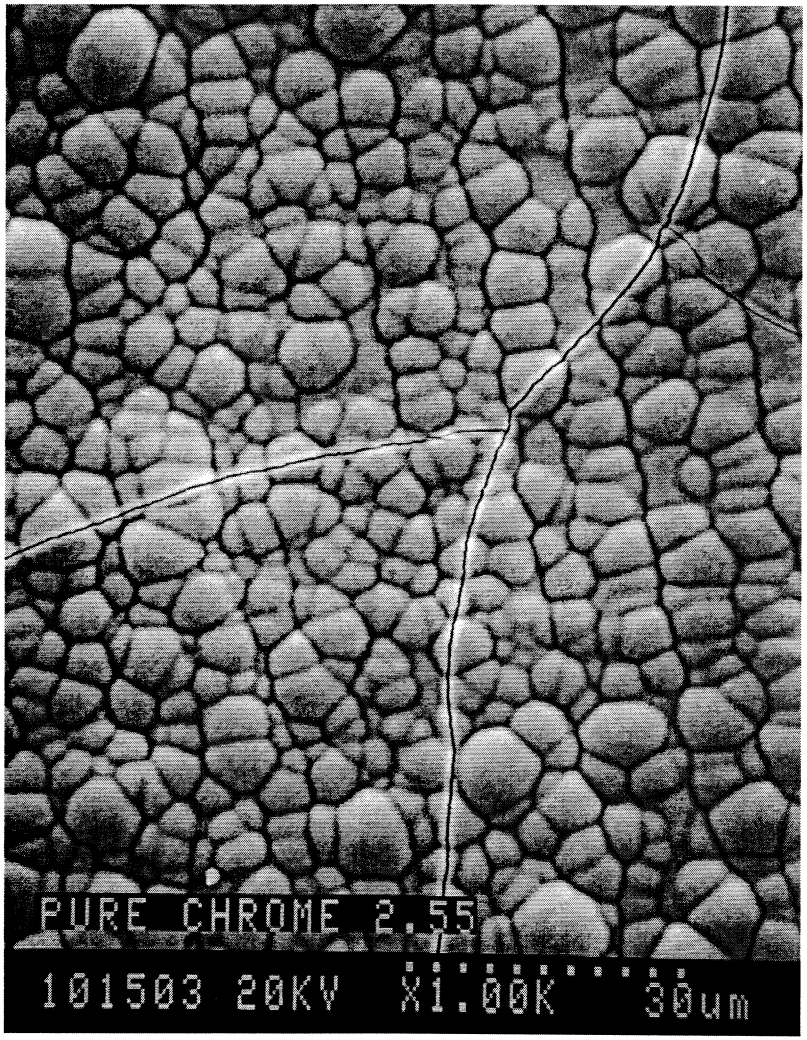

Figure 7: Micrograph of chrome plate deposited from pure hard chrome plating solution

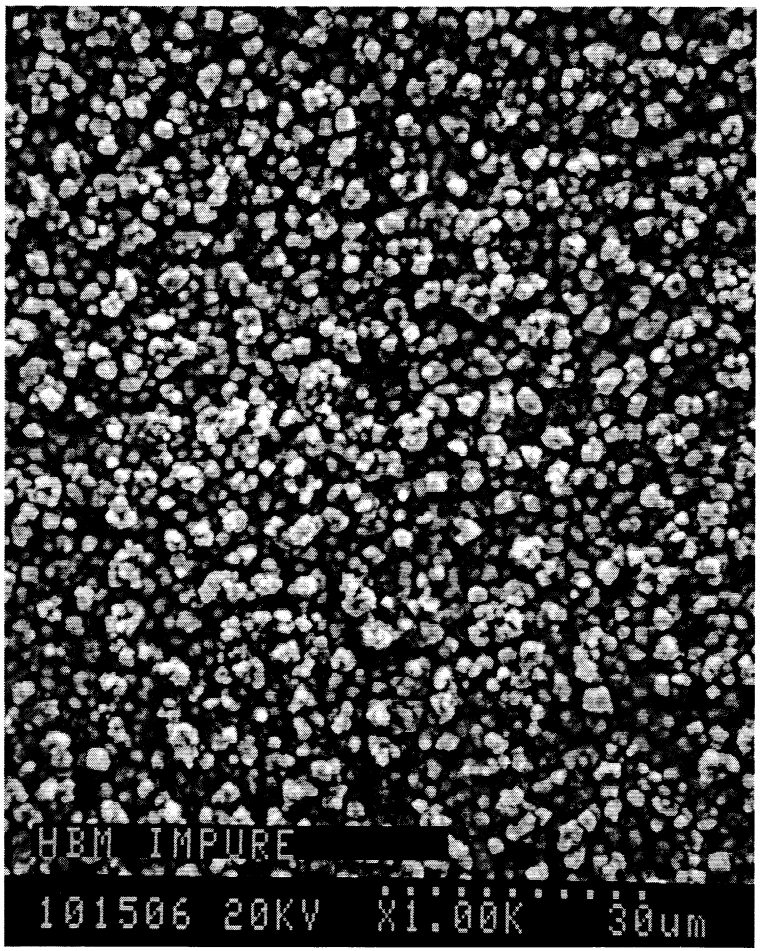

(a) impure

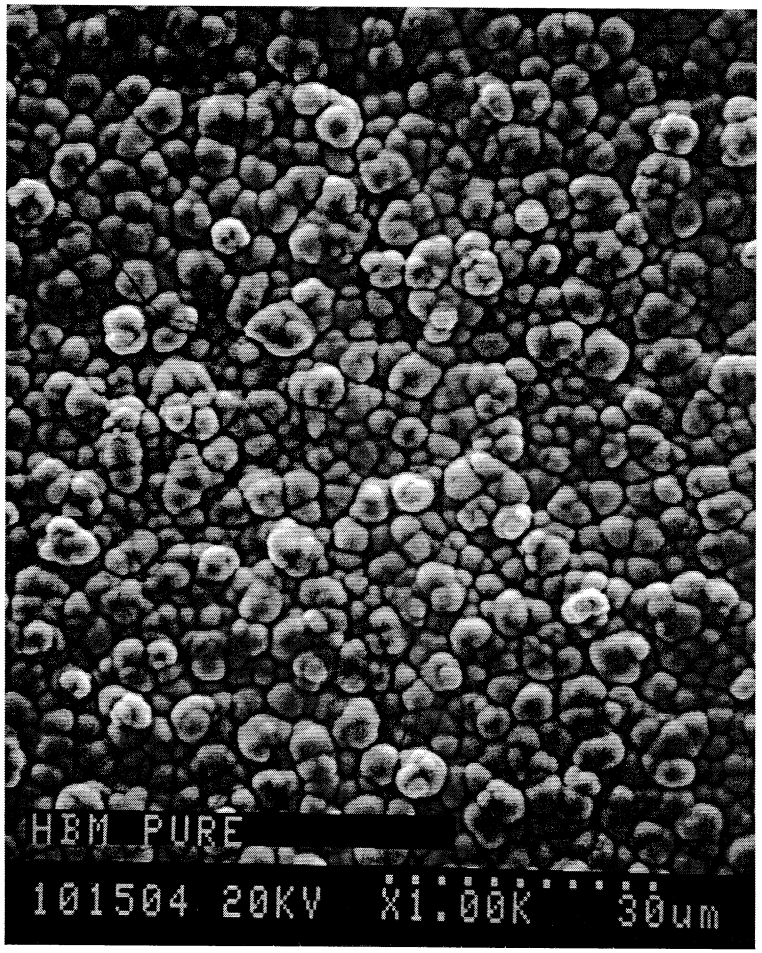

(b) rejuvenated

Figure8: Micrographs of chrome plates deposited from Set 1 solution

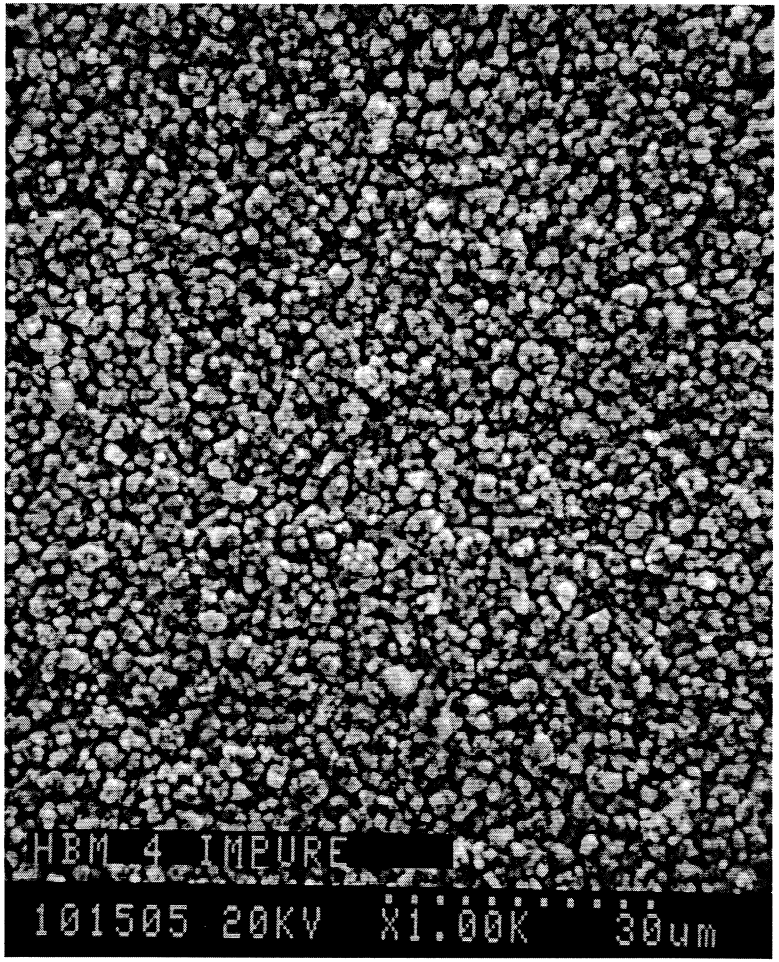

(a) impure

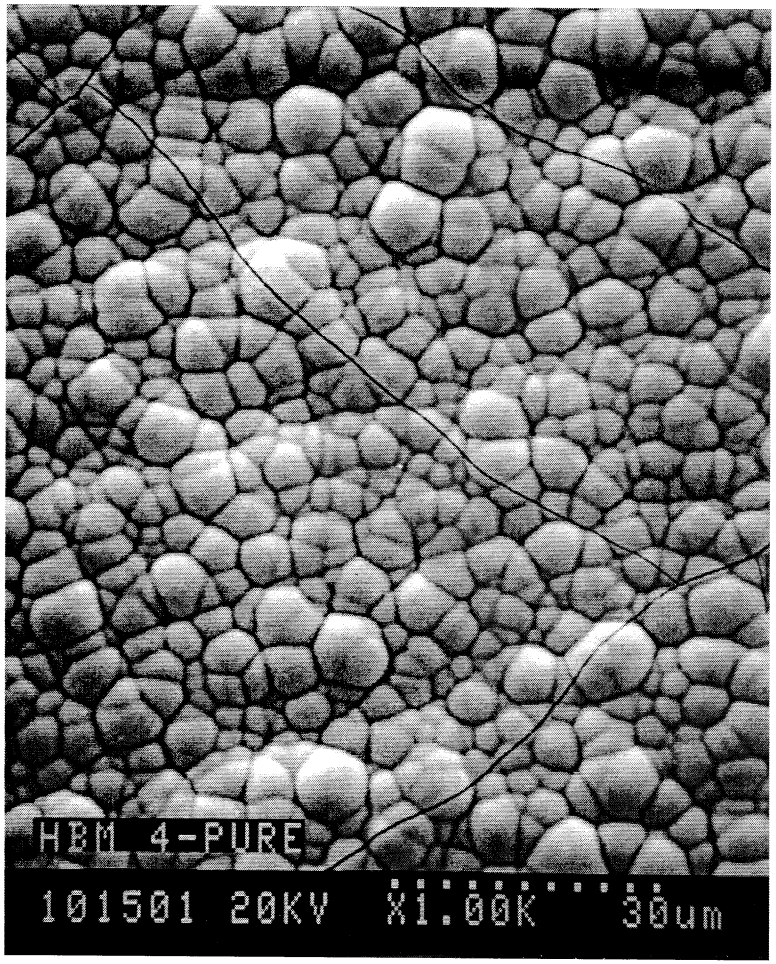

(b) rejuvenated

Figure 9: Micrographs of chrome plates deposited from Set 2 solution

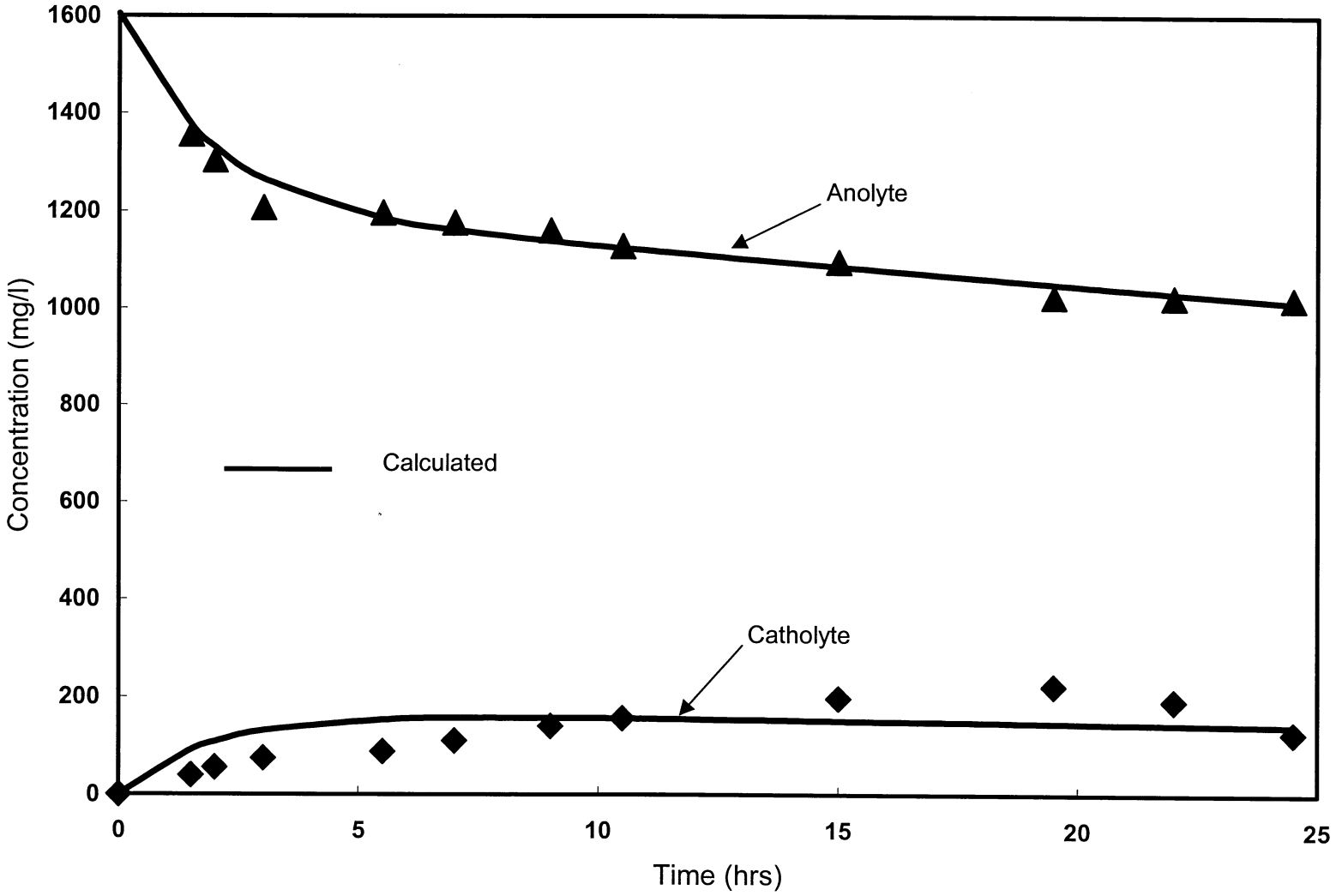

Figure 10 Concentration vs time for iron

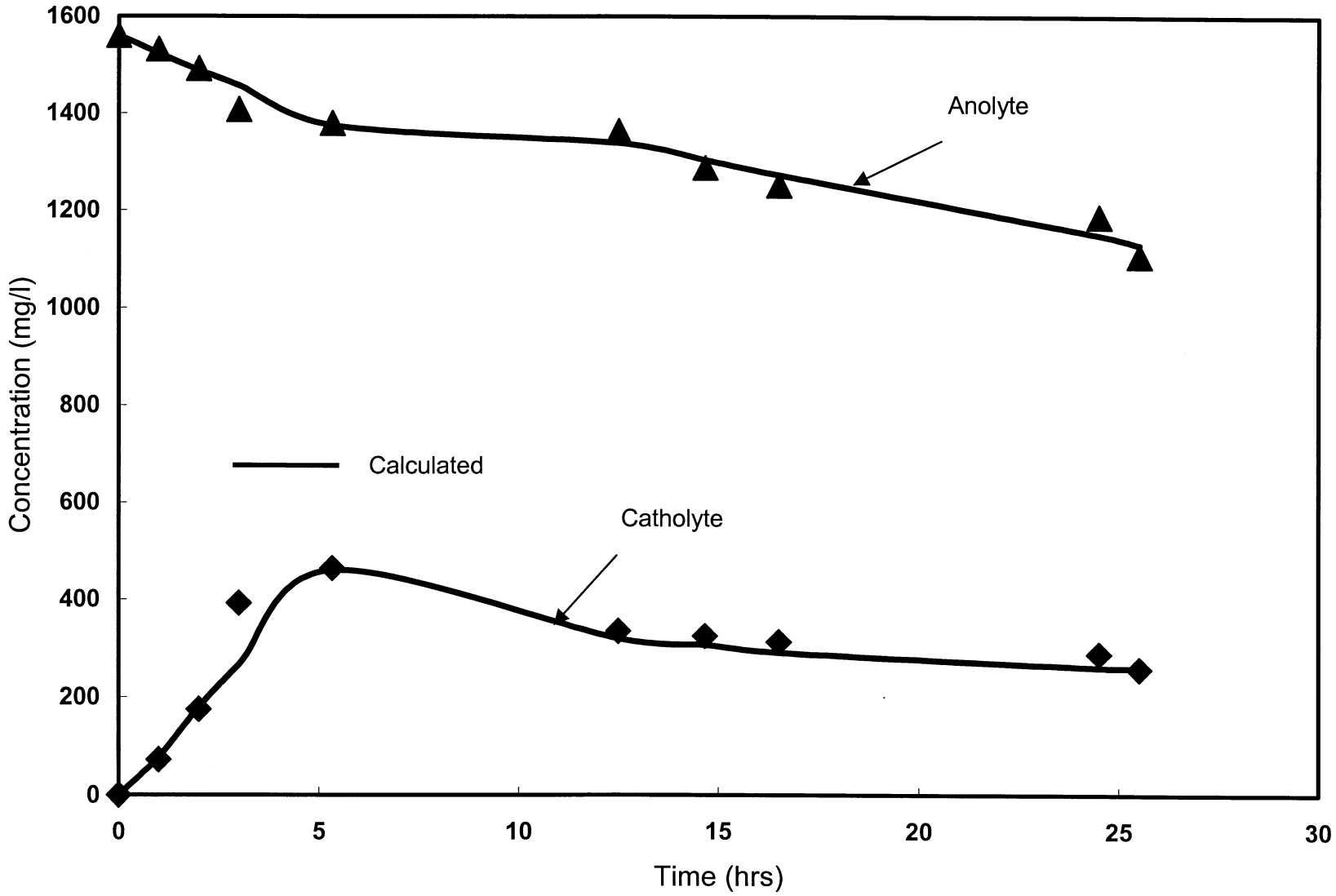

Figure 11 Concentration vs time for nickel

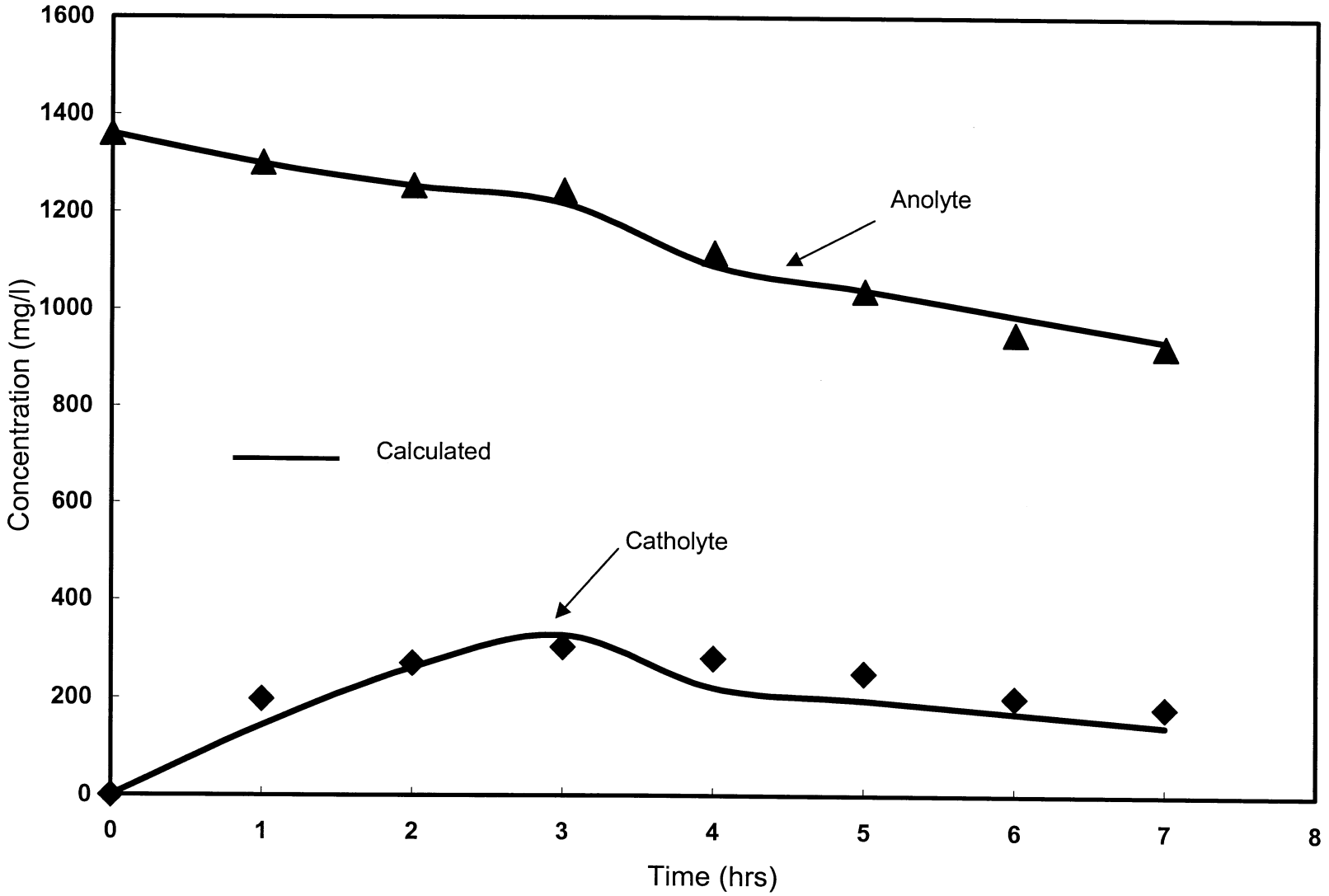

Figure 12 Concentration vs time for copper

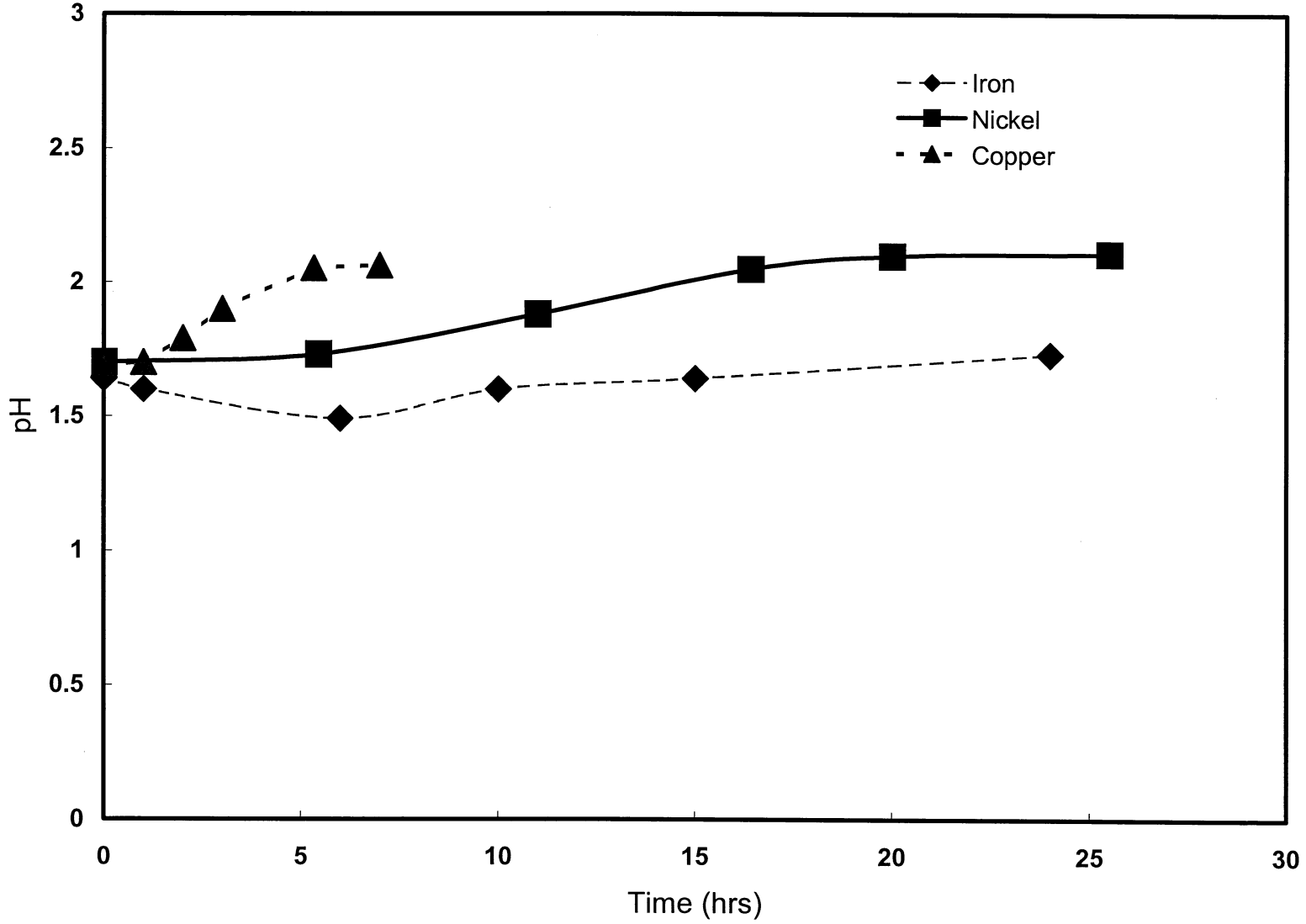

Figure 14 pH of catholyte vs. time

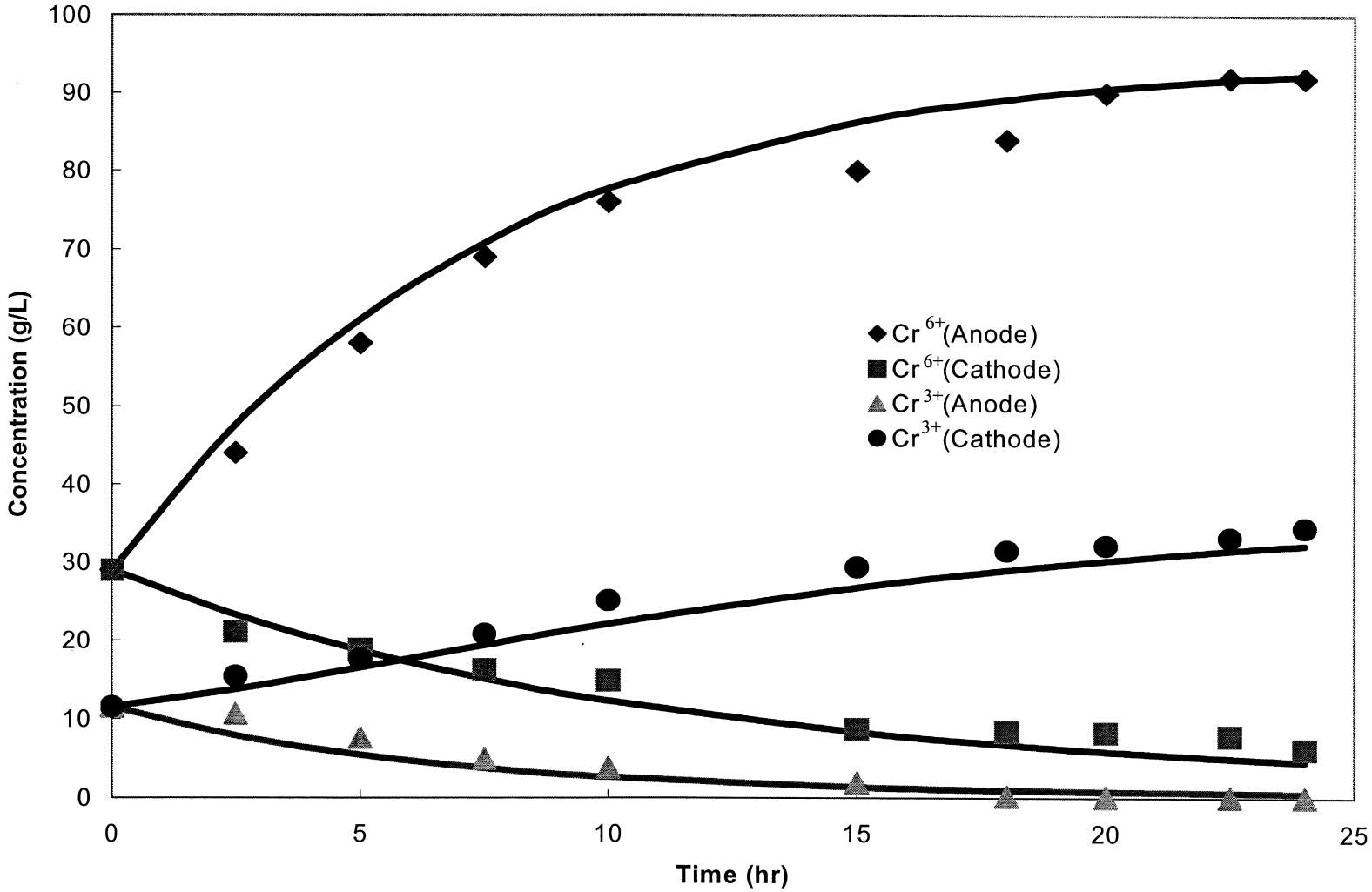

Figure 14 Concentration vs. time for chromium species in both compartments.
Initial concentration of hexavalent chromium of 29 g/l. Bi-doped lead dioxide anode was used.

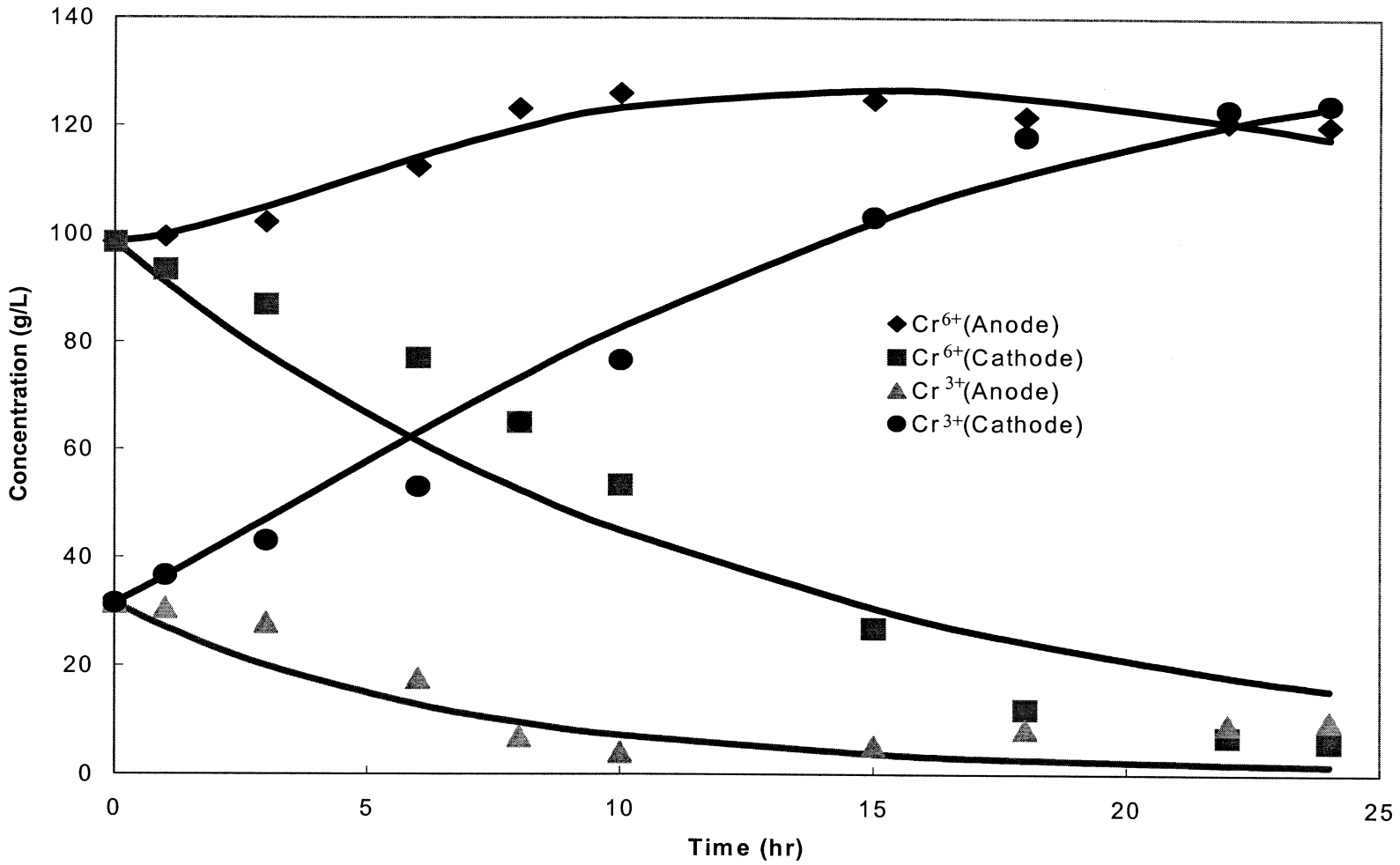

Figure 15 Concentration vs. time for chromium species in both compartments.
Initial concentration of hexavalent chromium of 98.5 g/l. Bi-doped lead dioxide anode was used.

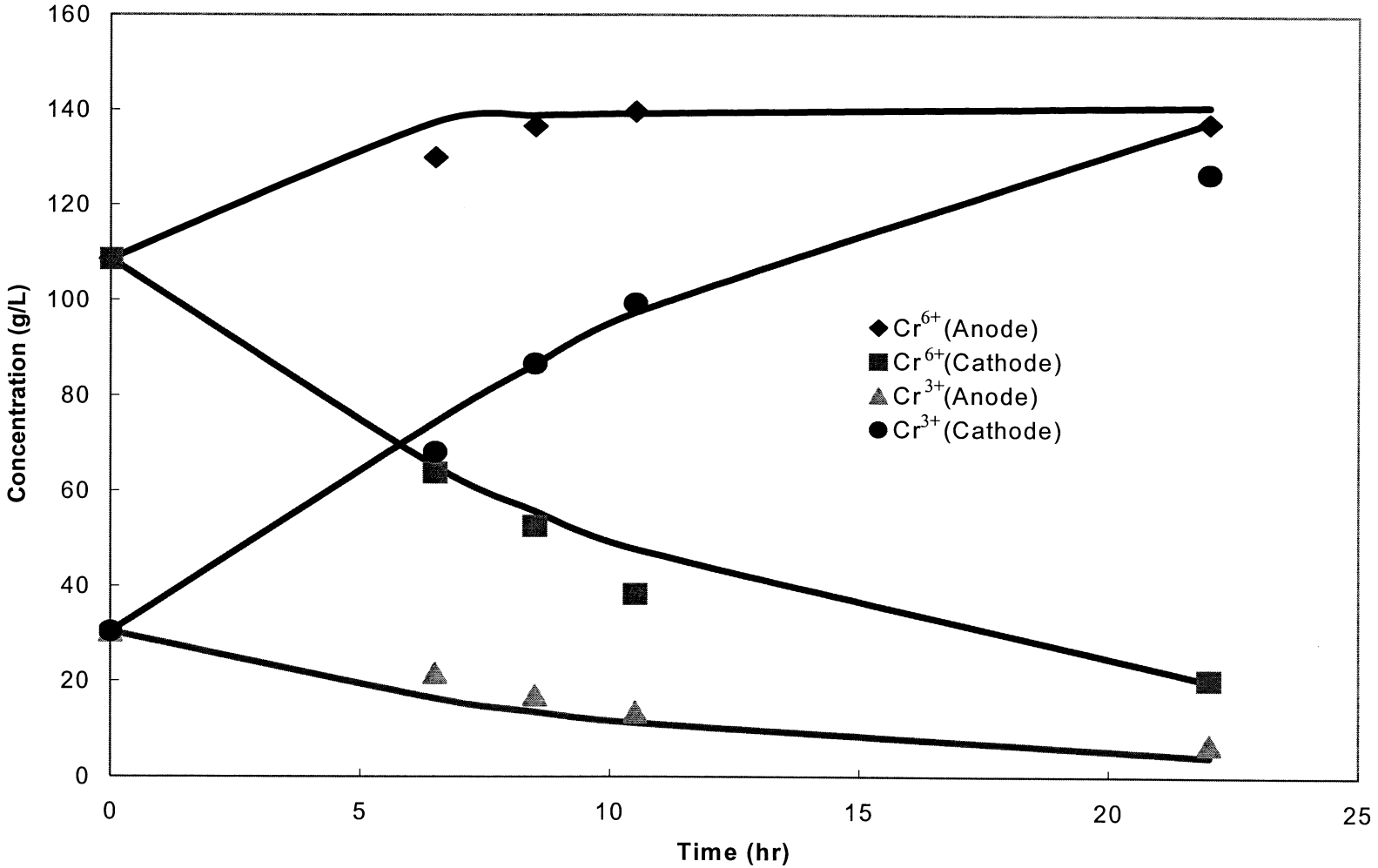

Figure 16 Concentration vs. time for chromium species in both compartments.
Initial concentration of hexavalent chromium of 108 g/l. Bi-doped lead dioxide anode was used.

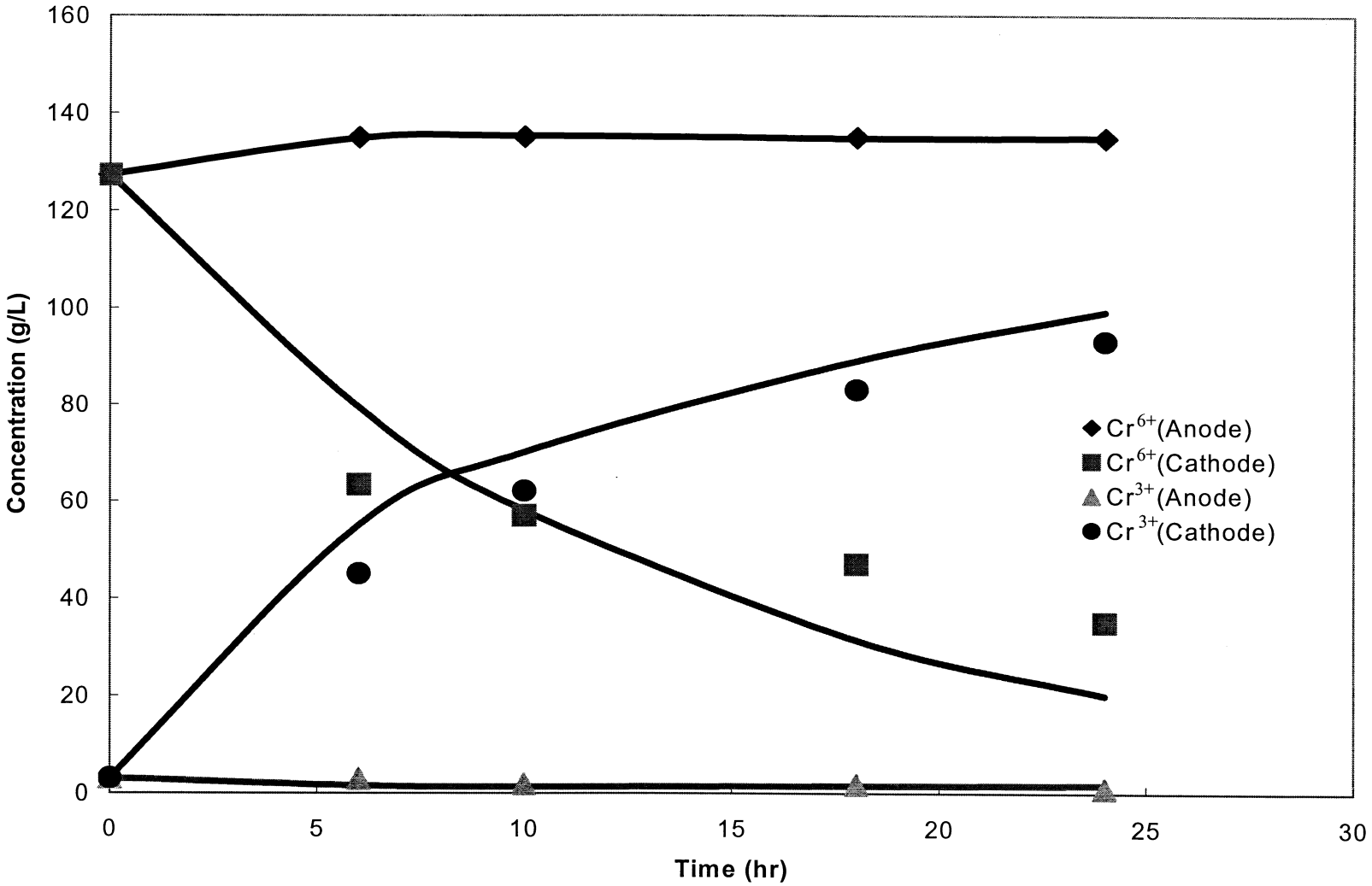

Figure 17 Concentration vs. time for chromium species in both compartments.
Initial concentration of hexavalent chromium of 127 g/l. Bi-doped lead dioxide anode was used.

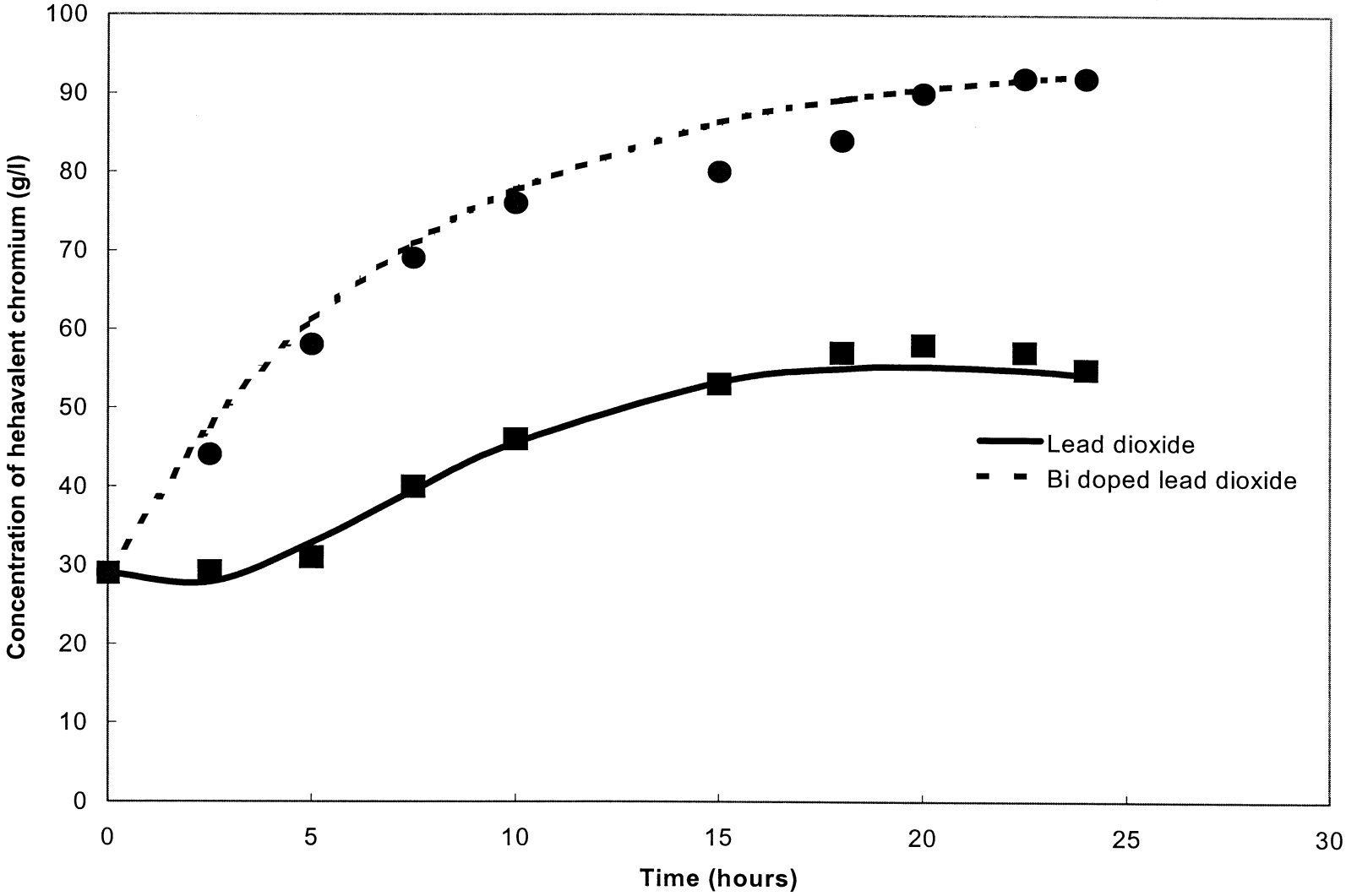

Figure18 Concentration vs. time for chromium species in anolyte.
Initial concentration of hexavalent chromium of 29 g/l.

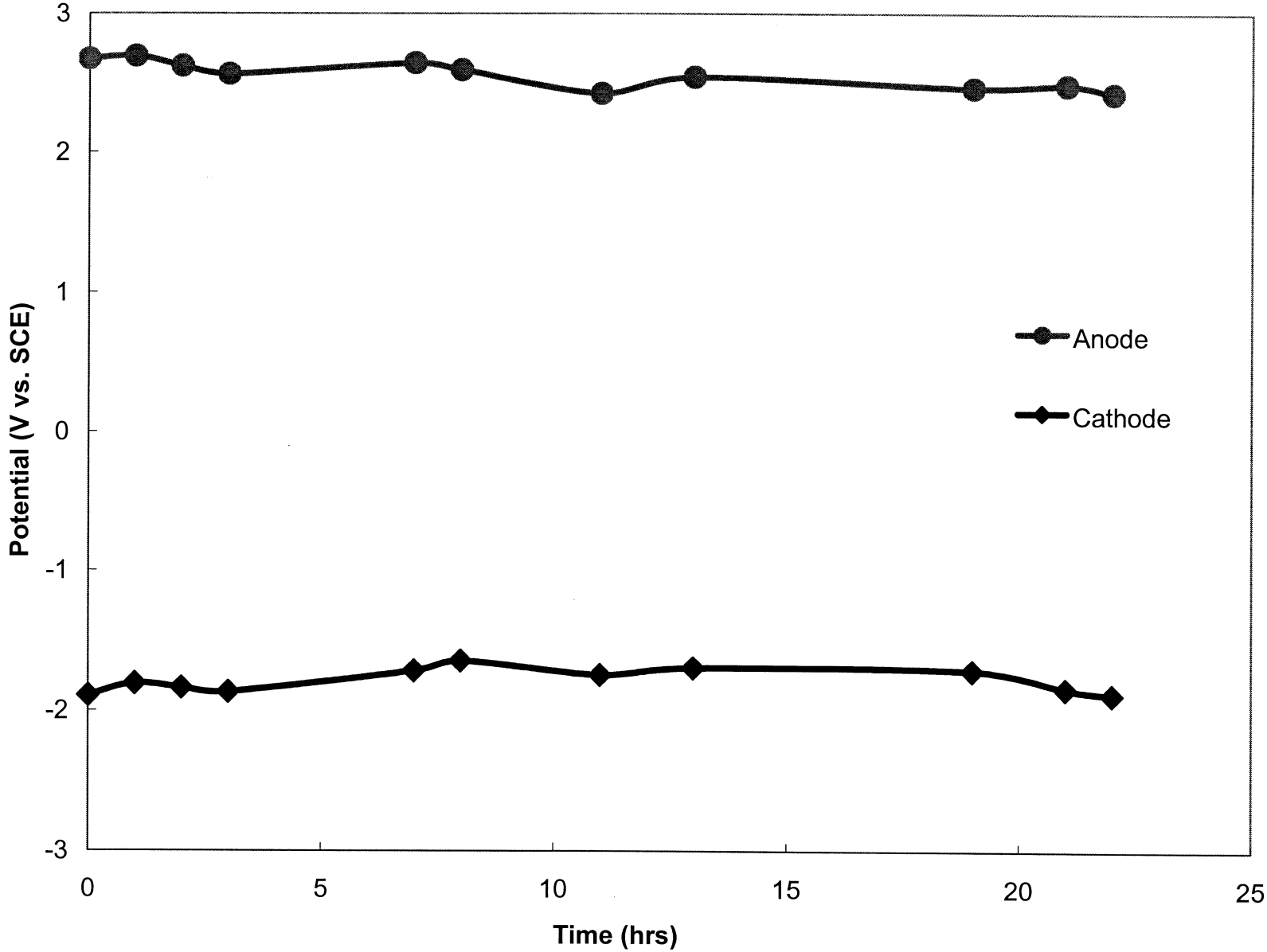

Figure 19 Potential (V vs. SCE) vs. time.

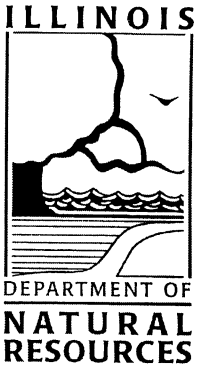
ILLINOIS
DEPARTMENT OF
NATURAL
RESOURCES